MINISTERE DE L'ENSEIGNEMENT SUPERIEUR ET DE LA RECHERCHE SCIENTIFIQUE

Felix Houphouet-Boigny University

UNITE DE FORMATION ET DE RECHERCHE SCIENCES DES STRUCTURES DE LA MATIERE ET DE TECHNOLOGIE

RÉPUBLIQUE DE CÔTE D'IVOIRE
UNION - DISCIPLINE - TRAVAIL

IME of RWTH Aachen University

N°: 669

SPONSORED BY THE Federal Ministry of Education and Research

MASTER

IN RENEWABLE ENERGY AND CLIMATE CHANGE

SPECIALITY: Production and Technology of Green Hydrogen

MASTER THESIS

Synthesis of Co-Fe powder using Ultrasonic Spray Pyrolysis and Hydrogen reduction

Presented on September 29th, 2023 by:

Saliha KEITA

MEMBERS OF JURY:

Prof. KOUADIO Yves	**PRESIDENT**
Dr.(MC) TILLUS Kessein Eric	**EXAMINER**
Dr (MC) KOUA Kamenan Blaise	**DIRECTOR**
Dr.-Ing. Srecko Stopic	**CO-DIRECTOR**

DEDICATION

I dedicate this master's thesis to my dear family. Their unwavering support, encouragement and sacrifice have been my constant motivation throughout this journey. Your trust in me gives me the strength to persevere, and your love is the foundation of my academic pursuit. Thank you for being there and understanding the long nights and countless hours of study we have had. This success is both yours and mine. My deepest gratitude for the love and guidance you have given me.

ACKNOWLEDGEMENTS

I would like to express my sincere gratitude to the following individuals and organizations who have contributed to the successful completion of my master's thesis:

- I am deeply thankful to BMBF and WASCAL for providing me with the scholarship that enabled me to pursue my master's degree and research.

- My heartfelt appreciation goes to the President of the University Abdou Moumouni for the guidance and support throughout the 1st and 2nd semesters of my studies.

- I extend my gratitude to the President of the University Felix Houphouet Boigny in Cote D'Ivoire for granting me the certificate upon the completion of my master's thesis.

- I would like to acknowledge the Vice Chancellor of the University of RWTH-Aachen in Germany, where I undertook my internship.

-I am thankful to the Director of WASCAL Niger at Abdou Moumouni University, Dr. RABANI Adamou, for the guidance and support during our stay for 1st and 2nd semesters.

- A special thanks to the Director of WASCAL/CEA-CCBAD Cote D'Ivoire at University Felix Houphouet Boigny Dr. KOUASSI Konan Edouard and Deputy Director Dr. KONE N'Golo for their valuable insights and mentorship greatly enriched my learning experience.

- A heartfelt thanks to the Director Prof. Bernd Friedrich of the Department and Chair for Process Metallurgy and Metal Recycling at RWTH-Aachen University for the guidance and support during my internship period.

- My appreciation goes to the Coordinator of the H2 Program and the Scientific Coordinator of WASCAL/CEA-CCBAD Cote D'Ivoire at University Felix Houphouet Boigny Dr. FASSINOU Wanignon Ferdinand and Dr. SORHO Fatogoma for his contributions to my academic journey.

- I would like to acknowledge my Major-supervisor, Dr KOUA Kamenan Blaise, for the valuable input and assistance that contributed to the quality of my research.

- I am deeply grateful to my Co- Supervisor, Dr.-Ing. STOPIC Srecko, for the continuous guidance, insightful feedback, and unwavering support throughout the entirety of my master's thesis.

- I extend my gratitude to the esteemed president of the jury Prof. KOUADIO Yves for his availability and his insightful question during my thesis defense.

- I would like to express my gratitude to Dr. TILLOUS Kessein Eric the jury examiner, for his expert insight into my document and thoughtful questions about my thesis.

- I would also like to acknowledge the dedication of the team members from Niger who were involved in the first and second semesters of my program.

- I extend my deep appreciation to my family, friends, and colleagues for their unwavering support that I have received so far.

- I extend my gratitude to Mr. Rosen Friedrich for all the support I received from him during my experiments in the laboratory.

I am truly appreciative of the collective efforts of these individuals and organizations, without whom this accomplishment would not have been possible. Thank you for your invaluable contributions to my academic journey and the successful completion of my master's thesis.

RÉSUMÉ

L'industrie automobile est en train de passer des véhicules traditionnels alimentés par des combustibles fossiles aux véhicules électriques. Ce changement s'inscrit dans le cadre de la transition énergétique croissante et peut accroître la demande de métaux vitaux tels que le nickel et le cobalt, essentiels à la production de batteries. En raison des problèmes liés à la production de cobalt à partir de sources primaires, le passage à des sources secondaires s'est imposé comme une évidence. Le recyclage est considéré comme une option alternative d'approvisionnement en extrayant le cobalt des ressources secondaires.

Dans cette étude, la synthèse de poudre de cobalt à partir de la solution de déchets industriels dérivée de la lixiviation d'un blanc de diamant polycristalline industriel à une température comprise entre 600 et 950 °C a été réalisée en utilisant la pyrolyse par pulvérisation ultrasonique et la méthode de réduction par l'hydrogène pour récupérer le cobalt. L'étude a comporté 21 cycles expérimentaux utilisant deux réacteurs distincts avec des temps de séjour variables (7,19 s et 23 s) et différents précurseurs : solution A (1,12 g/l de Co, 0,002 g/l de Fe), solution B (1,87 g/l de Co, 0,03 g/l de Fe), solution C (2,81 g/l de Co, 0,05 g/l). Les gouttelettes d'aérosol ont subi une réduction par l'hydrogène dans une plage de température de 600 à 950°C, ce qui a permis d'obtenir de la poudre de cobalt. Un débit volumétrique de 3 l/min (1 l/min Ar, 2 l/min H2) et un temps de réaction de 2 heures ont été utilisés. L'effet de la température de réaction, de la concentration de cobalt dans le précurseur, du temps de séjour et de la température sur la morphologie, la composition, la surface spécifique et la structure cristalline des particules de fer-cobalt synthétisées a été étudié, ainsi que la collecte des particules à l'aide d'un aimant.

Les résultats indiquent que des températures plus élevées entraînent une production accrue de cobalt. En outre, la modification de la concentration de cobalt dans la solution a influencé la taille des particules, montrant qu'une concentration plus élevée conduisait à des particules plus grandes. Un temps de séjour court (7,9 secondes) à 900°C s'est avéré plus approprié pour la synthèse de nanoparticules de cobalt, avec des particules sphériques allant de 191,1nm à 1222nm. Bien que le potentiel de collecte de poudre à l'aide d'un aimant soit évident, la récupération limitée de poudre de cobalt pourrait être attribuée à la concentration du précurseur ou à l'insuffisance de la force

magnétique. Malgré le succès de la capture de la poudre, il est crucial de relever le défi de la récupération de la poudre dans le tube.

Mots-clés : Production de cobalt, pyrolyse ultrasonique par pulvérisation, réduction de l'hydrogène, recyclage, sources secondaire

ABSTRACT

The automotive industry is transitioning from traditional fossil fuel-powered vehicles to electric ones. This change aligns with the growing energy transition and may raise demand for vital metals like nickel and cobalt, essential for battery production. Due to problems with cobalt production from primary sources, switching to secondary sources was the obvious choice. Recycling is seen as an alternative supply option by extracting cobalt from secondary resources.

In this study the synthetizes of cobalt powder from the industrial waste solution derived from leaching of industrial polycrystalline diamond blank at temperature range 600-950 C was performed using ultrasonic spray pyrolysis and hydrogen reduction method to recover cobalt. The investigation involved 21 experimental runs using two distinct reactors with varying residence times (7.19 sec and 23 sec) and different precursors solution A (1.12g/l Co, 0.002g/l Fe), solution B (1.87g/l Co, 0.03g/l Fe), solution C (2.81g/l Co, 0.05g/l). The aerosol droplets underwent hydrogen reduction within the temperature range of 600 to 950°C, yielding cobalt powder. The volumetric flow rate of 3 l/min (1 l/min Ar, 2 l/min H2) and a 2-hour reaction time were employed. The effect of the reaction temperature, the concentration of cobalt in the precursor, the residence time, and the on the morphology, composition, specific surface area, and crystal structure of the synthesized iron-cobalt particles was investigated also the collection of particle using magnet.

Results indicated that higher temperatures resulted in increased cobalt production. Furthermore, altering the cobalt concentration in the solution influenced particle size, showing that higher concentration led to larger particles. A short residence time (7.9 seconds) at 900°C was found to be more suitable for cobalt nanoparticle synthesis, with spherical particles ranging from 191.1nm to 1222nm. While the potential for powder collection using a magnet was evident, the limited cobalt powder recovery could be attributed to precursor concentration or magnetic strength insufficiency. Despite successful powder capture, addressing the challenge of powder recovery from the tube is crucial.

Keywords: Cobalt production, Ultrasonic Spray pyrolysis, Hydrogen Reduction, Recycling, Secondary sources

TABLE DES MATIÈRES

LIST OF FIGURES

LIST OF TABLE

LIST OF ABBREVIATIONS

EDS:	Energy Dispersive Spectroscopy
ICP-OES:	Inductively Coupled Plasma Optical Emission Spectrometry
IME:	Institut für Metallurgische Prozesstechnik und Metallrecycling
SEM:	Scanning Electron Microscope
USP:	Ultrasonic Spray Pyrolysis
XRD:	X-Ray Diffraction

INTRODUCTION

Today, in the automotive industry, the process of moving from the traditional production of vehicles with engines powered by the combustion of fossil fuels to vehicles powered by electric energy is underway. This revolutionary transformation comes at a time when the energy transition is growing and could increase demand for metallic raw materials such as nickel and cobalt, which are crucial for batteries [1].

According to [2] the abundance of critical minerals in Africa, including cobalt, lithium, copper, graphite, nickel, and rare earth minerals, places the continent in a favorable position to cater to the increasing demand of the global Electric Vehicle (EV) market. The cobalt market rebounded in 2021 growing 22% year-on-year (y/y) to 175 kt, demand will grow by 32 kt in 2021 alone, and by 51 kt over the five years between 2015 and 2020. Growth was driven by lithium-ion battery applications, which accounted for 63% of annual demand and grew 85% year-on-year [3]. Lithium-ion batteries are not only used in electric vehicles but also in personal electronic devices and as power storage for renewable energy sources like wind and solar, which are expanding areas of lithium-ion battery consumption.

Cobalt production harms the environment, particularly in areas with a high potential for this resource, such as the Democratic Republic of Congo, which has the world's largest cobalt reserves. The US Environmental Protection Agency has classified cobalt in the priority list of environmental risk elements as a potentially hazardous pollutant [4]**.** Due to political instability in the Democratic Republic of Congo (DRC), which supplies over 50% of global cobalt, there is uncertainty about future access to cobalt. Recycling is seen as an alternative supply option by extracting cobalt from secondary resources, given its critical raw material status [5].

In this particular study, the synthesis of cobalt powder from industrial waste solutions derived from the leaching process of industrial polycrystalline diamond blanks of the wire dies industry (Redies Deutschland GmbH) was conducted. The synthesis process involved employing ultrasonic spray pyrolysis and hydrogen reduction methods within a temperature range of 600 to 950°C. The primary aim was to recover cobalt from these waste solutions. The study encompassed a series of 21 experimental runs, utilizing two distinct reactors with varying residence times 7.19 seconds and

23 seconds alongside different precursor solutions, denoted as A, B, and C, each with varying concentrations of cobalt and iron. The obtained particles were analyzed by various methods. Particle morphology was characterized using scanning electron microscopy. The elemental composition of individual particles was investigated using energy dispersive X-ray spectroscopy. Crystallinity was confirmed by X-ray diffraction.

In view of the problems stated above, it is imperative to find the answers to the following question:

- How processing parameters can affect the final particles?
- What is the influence of the residence time on the structure of the particles?
- What is the effects of temperature in cobalt synthesis?
- Is the industrial waste better for cobalt recovery compared to synthetic cobalt solution?
- Can magnet optimize particle collection?

Based on the observations and background research conducted, we propose the following hypotheses as the focus of our research:

- Variation in processing parameters during USP-HR can lead to significant changes in the final particles
- The residence time has a direct influence on the behavior and properties of particles.
- Temperature has a significant impact on the outcome of cobalt synthesis
- The industrial waste solution based on cobalt is more effective than the synthetic cobalt solution in cobalt synthesis
- The use of a magnet can enhance particle collection efficiency

It will be discussed in this document three chapters:

- The chapter 1 named literature review details overview of cobalt resources, recovery of cobalt from primary materials and from secondary materials, Ultrasonic Spray pyrolysis Method, Characterization, Application of Iron-Cobalt, Magnetic properties of Iron-Cobalt, and Powder collection.

- The chapter 2 gives a comprehensive account of the Area study is presented, encompassing meticulous detailing of the methods, tools, and techniques deployed for data collection, data processing, and analysis.
- The chapter 3 encapsulates the outcomes of diverse analyses, such as SEM, EDS, and XRD, and examines the effects of various parameters, including temperature, concentration, and residence time, as well as different collection methods.

CHAPTER 1: LITERATURE REVIEW

This chapter is a detailed overview of cobalt resources, recovery of cobalt from primary materials and from secondary materials, Ultrasonic Spray pyrolysis Method, Characterization, Application of Iron-Cobalt, Magnetic properties of Iron-Cobalt, and Powder collection.

1.1 OVERVIEW OF COBALT RESOURCES

Cobalt is known by the chemical symbol Co and is one of the ferromagnetic transition metals in the d-block of group 9. It is listed in the periodic table of chemical elements between iron and nickel, with which it shares many physical properties [4]. Cobalt has an atomic number of 27, an atomic weight of 53.933194, a melting point of 1,495 ℃ (2,723 F), a boiling point of 2,870 ℃ (5,198 F) and a density of 8.9 g/cm3 at 20 ℃ (68 F**)** [6]. It is one of the least known metals and one of the rarest; its concentrations in crustal rocks average 25 ppm [7, 8]. The enrichment of cobalt in rocks occurs through various processes. It can increase concentration by a factor of 10, resulting in mineable resources. Natural cobalt is almost non-existent [7]. It is mostly found in certain sulfides, selenides, arsenides, sulfur arsenides, carbonates, sulfates, and arsenates. There are 34 known cobalt minerals. Some of the best-known are cobalt, rhodochrosite (MnCO3), and carrollite (CuCo2S4). It may also be present in hydrous oxides, such as absolane, or sulfides known as cobalt pyrites [7, 8].

Cobalt is formed as a by-product of other metals such as copper and nickel, and the major source of cobalt in recent decades has been nickel. It has been reported by [9] in 2015, that the world's terrestrial cobalt reserves are approximately 8.3 million tons. They are primarily distributed in the Democratic Republic of the Congo, Australia, Indonesia, and Cuba. These countries contain 75% of the world’s total reserves and 48% of the Democratic Republic of the Congo. In 2018, the Democratic Republic of Congo emerged as the primary global cobalt producer, accounting for more than 71 percent of the total 126,000 tons mined. The remaining 22 percent of cobalt production was distributed relatively evenly among several other countries, namely Russia, Cuba, Australia, the Philippines, Canada, and Madagascar (Figure 1) [10].

Regarding global cobalt reserves, the significance of the DR Congo becomes even more evident. Out of the approximately 7.4 million tons of economically exploitable cobalt reserves worldwide,

nearly 48 percent is situated in this Central-African nation. Australia comes in second with 17 percent, followed by Cuba with 7 percent, while several other countries hold smaller proportions, each below 5 percent (Figure 2). Today, after 20 years, the Democratic Republic of Congo (DRC) is back at the forefront of copper and cobalt production [11].

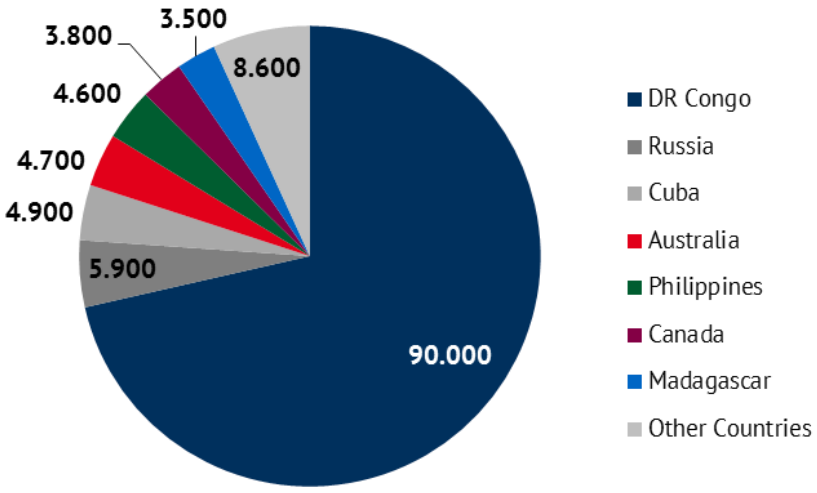

Figure 1: Estimated cobalt mining in 2018 [10]

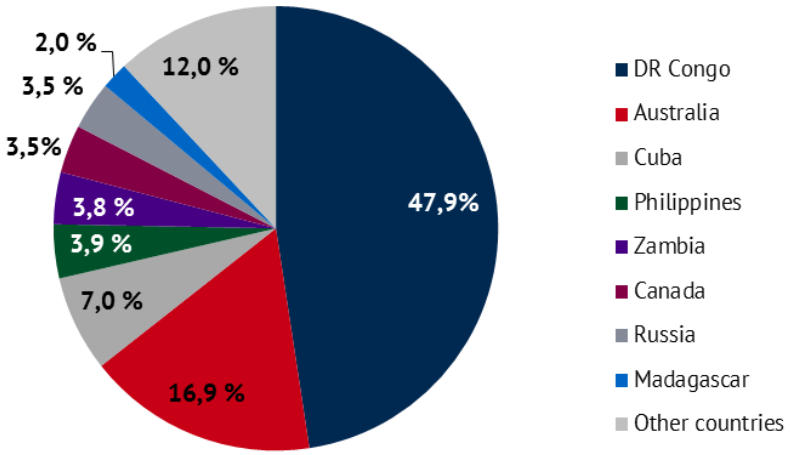

Figure 2: shares of global cobalt reserves [10]

1.2 RECOVERY OF IRON-COBALT

1.2.1 Recovery of Cobalt From Primary materials

Nickel-cobalt-bearing laterites have an average grade of 1.3% Ni and 0.04% Co, with a total tonnage of 56 million tonnes. Middle-grade Ni deposits exceed 1.5% Ni, while high-grade Ni deposits contain over 1.8% Ni [12]. Laterite ores are now the primary global source of nickel and cobalt. While pyro metallurgical processing remains dominant, hydrometallurgical technologies are increasing in producing nickel and cobalt. Hydrometallurgy offers lower energy demands, operational costs, and environmental impacts [13]. According to [14] the process achieved high recovery rates: over 91% for cobalt and 84% for copper from cobaltite concentrate. It involved oxidative pressure leaching, jarosite precipitation, ferric arsenic precipitation, selective solvent extraction for copper, and electro winning for both copper (99.89% pure) and cobalt (99.8% pure) (Figure3).

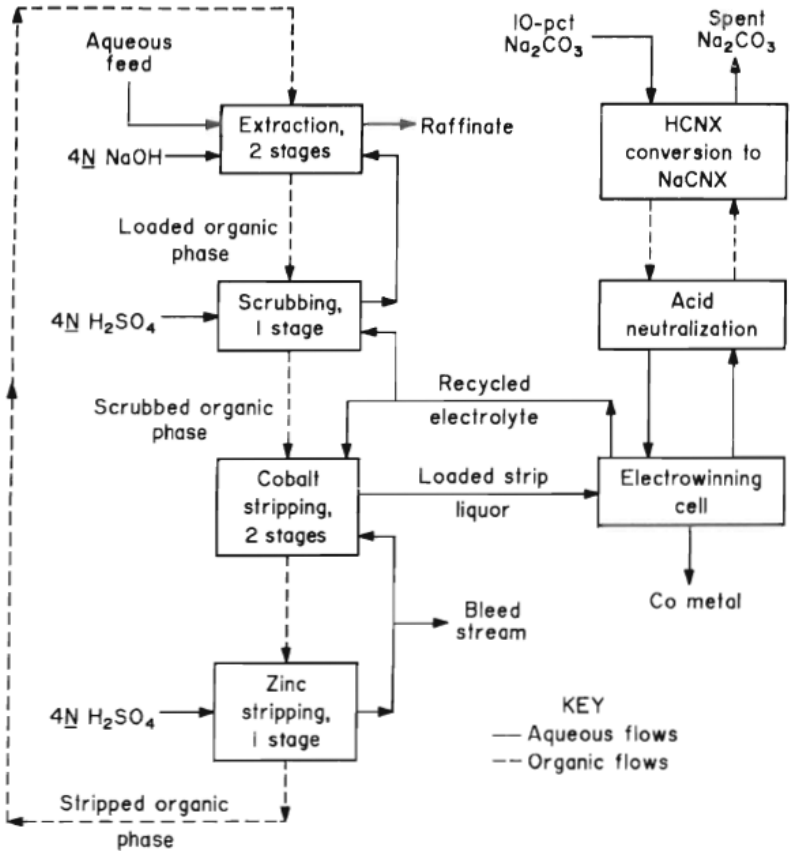

Figure 3: Conceptual flow diagram for cobalt solvent extraction and electrowinning [14]

1.2.1.1 Leaching of Copper, Cobalt, and Nickel from Complex Ore

Yotamou et al,.[15] studies leaching of complex copper–cobalt–nickel ore from Mwinilunga, Zambia. Optimal conditions for leaching were found as follows: 65–75 °C temperature, 1-hour time, and 0.6 wt% sodium metabisulphite (SMBS) addition. Copper, cobalt, and nickel were recovered via precipitation with sodium sulphide and magnesium oxide, with sodium sulphide showing higher selectivity. SMBS addition dissolves Cu, Co, and Ni (Table 1). Above 0.6% weight, recovery doesn't improve (Table 2).

Table 1: Leach test results showing effect of pH and temperature on % recovery. Samples leached [15]

pH	SMBS (wt%)	% Recovery				Acid consumption (kg/ton ore)
		Cu	Co	Fe	Ni	
(a)						
pH = 1.4	1.0	81.58	88.57	36.10	70.00	138
pH = 1.6	1.0	74.91	88.57	20.75	58.46	106
pH = 1.8	1.0	70.18	81.90	14.11	58.46	67
pH = 2.0	1.0	74.21	81.90	17.84	61.54	40
(b)						
pH = 1.4	1.0	55.92	71.82	1.754	29.23	74
pH = 1.6	1.0	58.78	73.00	0.439	31.54	72
pH = 1.8	1.0	53.06	77.27	4.825	30.77	69
pH = 2.0	1.0	51.84	85.91	0.877	34.62	39

Table 2: Leach test results showing the effect of SMBS addition. Samples leached at 70 °C in (a) [15].

pH	SMBS wt%	% Recovery				Acid consumption (kg/ton ore)
		Cu	Co	Fe	Ni	
(a)						
pH = 1.8	0	27.52	16.32	6.93	12.04	36
pH = 1.8	0.6	74.74	80.48	15.77	65.38	84
pH = 1.8	1.0	70.18	81.90	14.11	58.46	67
pH = 1.8	1.5	77.89	87.62	30.29	63.85	69
pH = 1.8	2.0	76.32	86.67	34.44	66.15	74
(b)						
pH = 1.8	0	21.83	13.29	0.94	8.34	18
pH = 1.8	0.6	56.33	61.82	1.75	38.46	32
pH = 1.8	1.0	53.06	77.27	4.82	30.77	69
pH = 1.8	1.5	56.33	70.45	4.83	43.08	44
pH = 1.8	2.0	59.18	78.64	7.02	36.92	32

1.2.1.2 Nickel and cobalt extraction from laterite ore via carbothermic reduction roasting-ammoniacal leaching.

Carbothermic reduction roasting and ammoniacal leaching of Ni-laterite ore from Bajaur (Pakistan) were studied by [16] for potential Caron process exploitation. Plenty of available coal replaced costly fuel oil. Optimal conditions were 10 wt% coal, 9 wt% Na2SO4, roasting at 800 °C for 120 min.

Table 3: Chemical composition of Ni-laterite and coal sample[16].

(a) Laterite ore	Contents	Fe total	Ni	Co	Mn
	Wt.%	47.12	1.43	0.16	0.65
(b) Coal	Contents	Fixed carbon	Ash	Volatile matters	Sulfur as S^0
	Wt.%	58.6	8.6	27.1	7.5

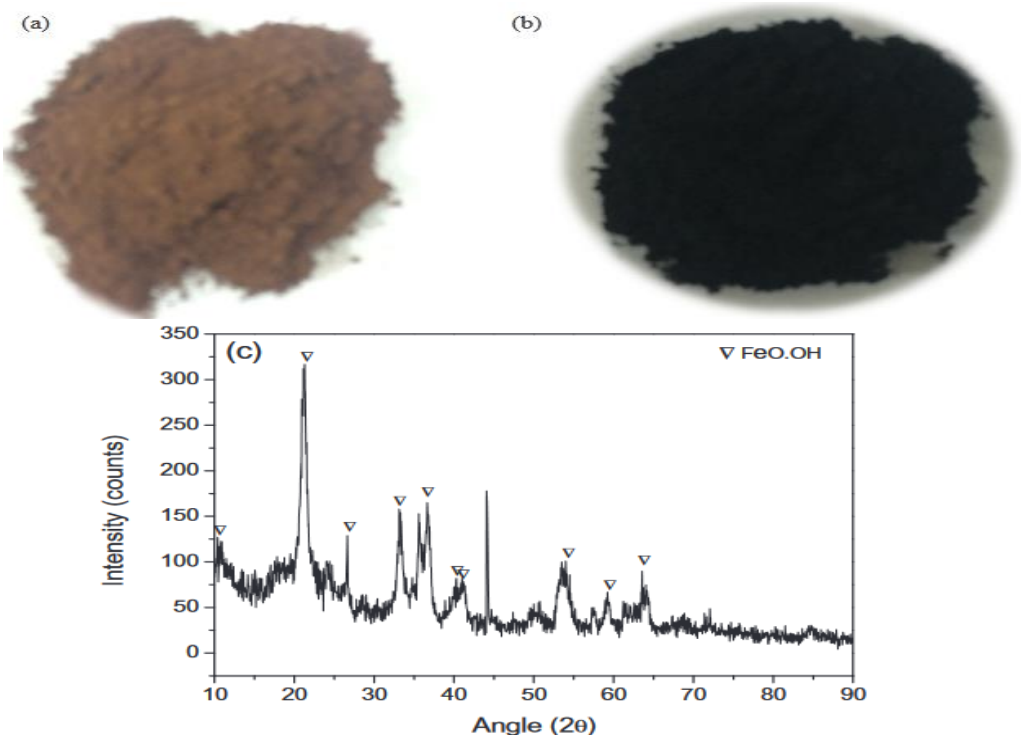

Figure 4: The ground sample of nickel laterite ore (a), coal of size −100 μm (b), an XRD patterns of Ni-laterite sample used in this study (c) [16].

Leaching with NH4OH–(NH4)2CO3 yielded > 90% Ni, 67% Co. Selective extraction of > 97% Ni over Co using LIX 84-I at 1:10 organic-to-aqueous ratio. The Caron process can be technically feasible for Ni and Co extraction from Bajaur lateritic ore.

1.2.2 Recovery of Iron-cobalt from secondary materials

Cobalt-bearing secondary resources, including end-of-life products, processing waste, and various metallurgical byproducts like waste catalysts, magnets, superalloys, cemented carbides, and rechargeable batteries, and others, play a pivotal role in recycling. This process fosters a transition to a more circular economy, particularly due to the uncertainty surrounding primary cobalt supply and its critical raw material status, making improved recycling and recovery of cobalt increasingly vital[5].

1.2.2.1 From Waste catalysis

Chandra et al. [5] Reports that the acid leaching with H2SO4 is efficient for cobalt and molybdenum, and alkali leaching is less effective. Metal recovery is achieved through solvent extraction or precipitation. Pyrometallurgical processes involve calcination smelting, and pyro-hydrometallurgical methods include alkali roasting and chlorination roasting combined with leaching. Biohydrometallurgical processes with microorganisms like Acidithiobacillus ferrooxidans and Acidithiobacillus thiooxidans explore cobalt leaching from spent catalysts.

Sivasakthi and Sathaiyan [17] Studied the recovery of cobalt from a waste catalyst in the petroleum refining industry by using a hydrometallurgical process Figure 5. The process involves roasting the catalyst with flux material at 700°C, leaching with sulfuric acid, and precipitating cobalt at pH 12 with NaOH. After filtering and dissolving the cob alt hydroxide, a cobalt sulfate solution is obtained for electrolytic recovery Optimization of parameters and SEM characterization are performed. The process yields a compact metallic deposit with 70% cobalt content (Table 4). The same process has been used by Wolańczyk et al. [18] for recovering cobalt (II) from solutions after leaching spent industrial catalysts used in the hydrodesulfurization process. A four-stage process is proposed Figure 6, showing successful leaching of Co(II) and Mo(VI), removal of main impurities (Al(III) and Fe(III)) during hydroxide precipitation, and efficient Co(II) separation from Mo(VI) through extraction and stripping (Table 5).

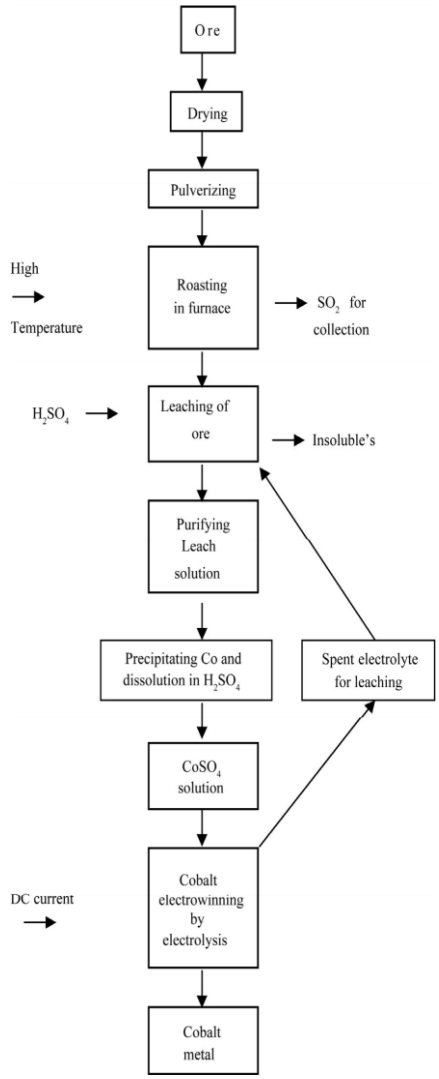

Figure 5: Flow chart on cobalt[17].

Table 4: Optimum electrowinning parameters[17].

Different parameters		Weight of cobalt deposit (gm)	Current efficiency (%)
H_2SO_4 concentration	5 g/L	0.8031	61.5
Duration	120 min	0.8031	61.5
Cobalt concentration	30 g/L	0.8031	61.5
Current density	200 A/M^2	0.7320	85.1
Temperature	30 °C	0.7320	85.1
Stirring	Nil	-	-

Figure 6: Four-step process for hydrometallurgical recovery of Co(II) from CoMo catalyst of hydrodesulfurization[18].

Table 5: Recovery yield of Co(II) and Mo(VI) in the four-step process (leaching-precipitation-extraction-stripping)[18]

Temperature of Leaching with 0.5 M H_2SO_4, °C	Concentration in the Leach Solution, g/dm^3		Concentration in the Stripping Solution, g/dm^3		Y, %	
	Co(II)	Mo(VI)	Co(II)	Mo(VI)	Co(II)	Mo(VI)
23	0.81	3.97	1.93	0.07	16.5	0.08
55	0.90	4.49	2.22	0.05	18.6	0.07
75	0.99	5.45	2.53	0.07	19.8	0.12
95	1.11	6.06	3.63	0.34	18.8	0.33

1.2.2.2 From Lithium ions Battery

The recycling process for lithium-ion batteries (LiBs) waste begins with pre-treatment procedures, involving physical/chemical separation, including mechanical and chemical/thermal termination processes[19, 21]. Various chemical approaches have been utilized in the recycling process, including chemically induced precipitation, solvent extraction, electrochemical systems, pyrometallurgical, and hydrometallurgical methods[22, 24]. While hydrometallurgical processes have been commonly recognized for their distinct stages of pre-treatment, subsequent leaching, and eventual metal separation[22].

According to Chandra et al. [5] the pyrometallurgical process allows direct smelting of spent LIBs but has higher energy consumption and potential pollution. It needs to be combined with hydrometallurgy to recover metals from slag. Hydrometallurgical processing using acid and alkaline solutions is researched for high selectivity and low-energy requirements. Ammonia leaching shows promising results. Methods like precipitation and solvent extraction are used for further metal recovery. Bio-hydrometallurgy is cost-effective and eco-friendly but has drawbacks in operation time and control. Figure 7 provides a concise overview of cobalt recycling possibilities.

The exploration of metal recovery from spent Li batteries, encompassing elements such as Co, Li, Zn, and Mn ions, represents an alluring field of research owing to the substantial volume of their waste. Numerous extraction methods have been suggested for battery recycling, among them being the pyrometallurgical/hydrometallurgical processes[25, 27]. A novel hydrometallurgical process has been developed for recovering pure cobalt sulfate solution from waste cathodic material in

lithium-ion battery manufacturing. Leaching was optimized based on various factors, achieving 93% cobalt and 94% lithium leaching. Subsequent solvent extraction yielded 85.42% cobalt recovery using 1.5 M Cyanex 272 at an organic phase to aqueous phase (O/A) ratio of 1.6 and pH 5.00. The remaining cobalt was fully recovered using 0.5 M Cyanex 272 at an O/A ratio of 1 and pH 5.35. Co-extracted lithium was scrubbed with 0.1 M Na2CO3. Finally, a 99.99% pure cobalt sulfate solution was obtained via H2SO4 stripping of the cobalt-loaded organic[28].

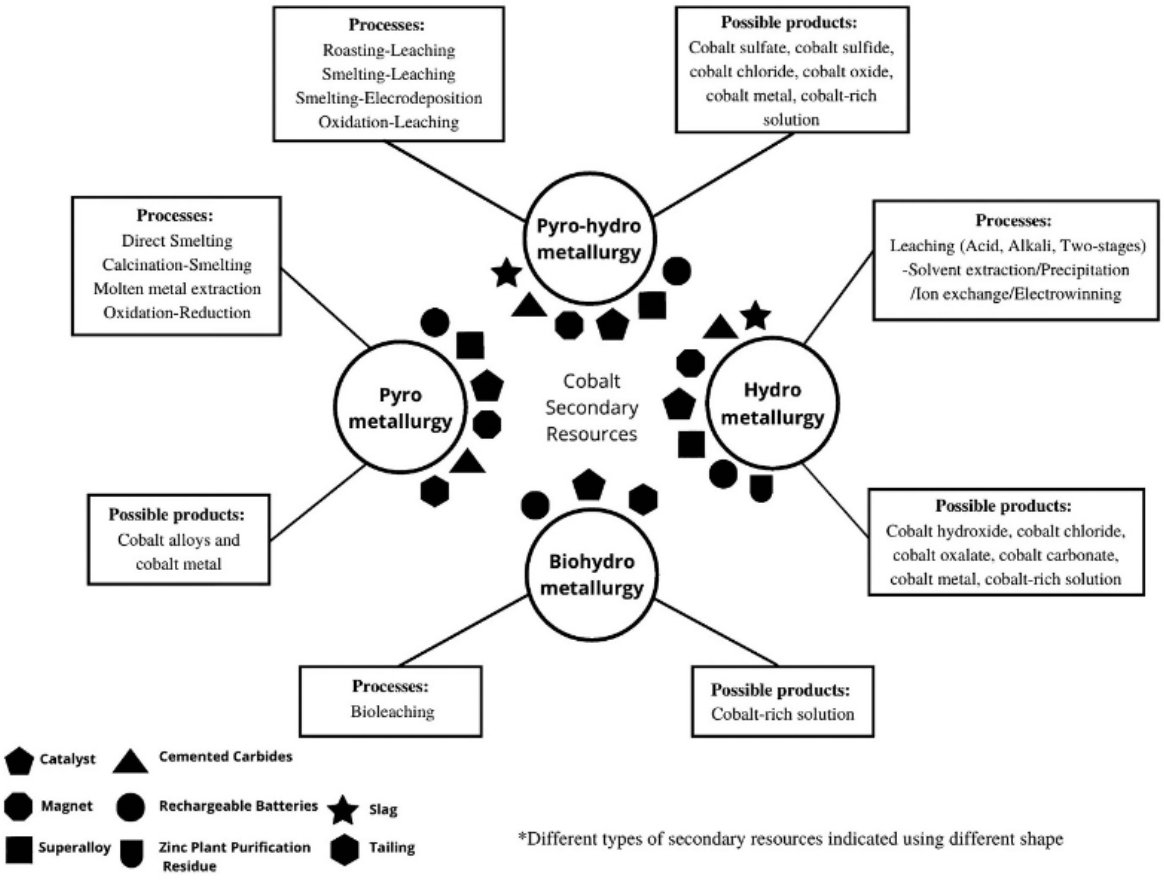

Figure 7: Summary of cobalt secondary resources with their respective recycling processes

1.2.3 From Cemented tungsten carbide

Stopić and Friedrich [14] Utilized ultrasonic spray pyrolysis in a hydrogen atmosphere to produce cobalt from cemented tungsten carbide, with a chemical composition of 75.86% W, 8.14% Co, and 6.07% C. The fraction below 90 μm underwent nitric acid treatment, and the resulting leach solution was used for cobalt production. The final cobalt concentration reached

0.08 mol Co/l. Controlling the reaction temperature determined the size of the cobalt powder, yielding spherical particles with a mean diameter below 500 nm at 800°C using 0.4 mol/l cobalt nitrate. Byun et al. [29] Reports tungsten and cobalt can be efficiently recovered from cemented tungsten carbide-Co scraps through a novel roasting and water-leaching process with Na2CO3. The optimized conditions achieve over 95% W recovery and over 94% Co recovery as soluble CoSO4, producing a high-purity Co hydroxide product (>99.5% purity) with minimal impurities.

The low-temperature acid aqueous electrochemical method efficiently recovers tungsten and cobalt from spent cemented carbide, minimizing pollution and energy consumption. The process as showing in Figure 8 shows high efficiency and offers favorable conditions for recovering other valuable metals from spent alloys[30].

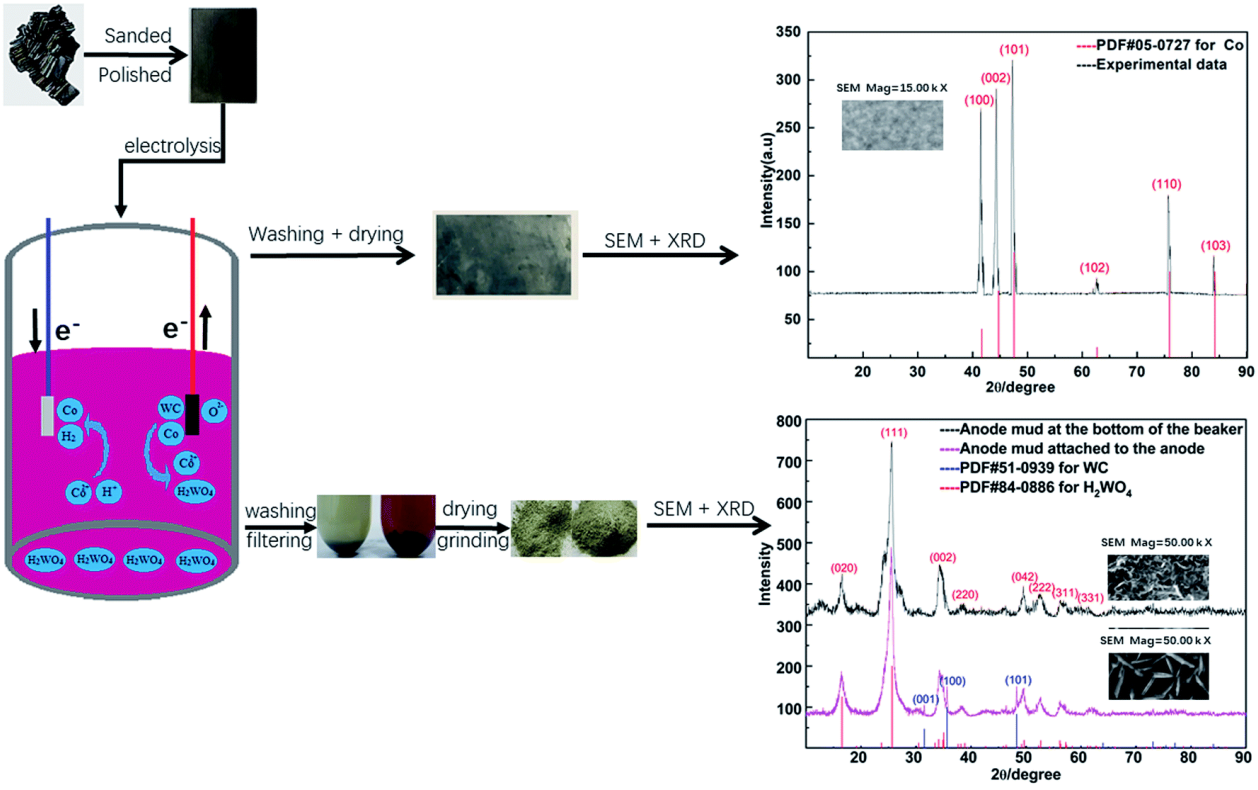

Figure 8: Experimental process[30].

Molten salt electrolysis successfully separates and recycles tungsten and cobalt from cemented carbides. Electrochemical techniques reveal reversible reduction reactions controlled by ion diffusion, yielding pure cobalt and WC powder (>90% purity) from WC–6 wt% Co scrap[31].

1.2.4 From Polycrystalline Diamond

Ultrasound-assisted leaching of industrial polycrystalline diamond (PCD) blanks in aqua regia (60-80°C) enhances cobalt (20 wt.%) removal for cost-effective PCD reuse. Kinetic models, including thermochemical aspects, were used to study cobalt dissolution. Optimal conditions involved low solid/liquid ratio and full ultrasound use. A transition from a reaction-controlled to diffusion-controlled shrinking core model occurred for PCD thickness > 2.8–3.4 mm. Intermittent ultrasound doubled the reaction rate constant, while continuous ultrasound increased it 1.5-fold. The activation energy for leaching 5 μm grain size PCD ranged from 60-80°C was 20 kJ/mol [32]. The SEM image is showing in Figure 9. EDX is shown in Table 6.

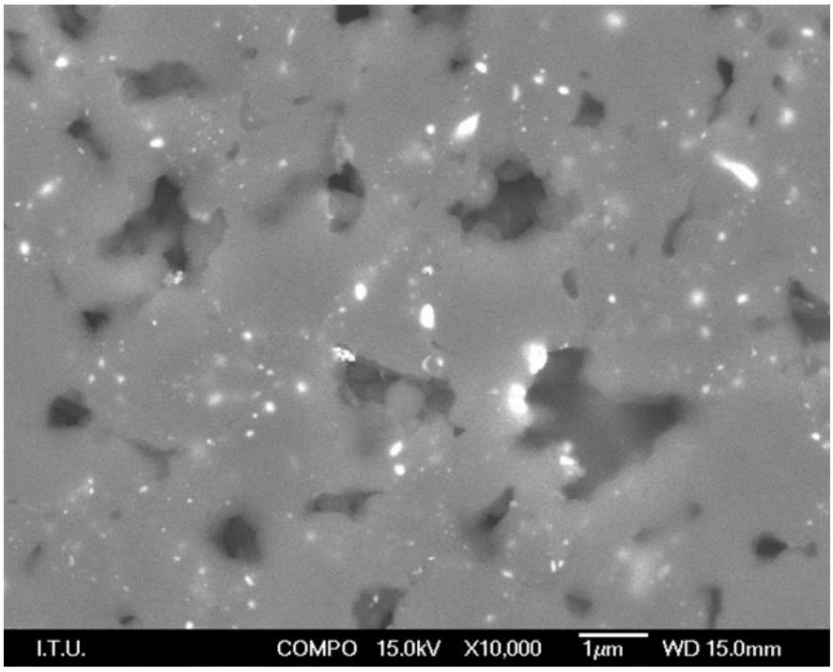

Figure 9: SEM image of ground and polished PCD surface, 5 μm class (dark grey areas are the bridged diamond grains with cavities where traces of cobalt also show up as lighter shades) [32]

Table 6: Energy dispersive X-ray spectroscopy image of ground and polished PCD surface, also 5 µm class[32].

Content (Weight %)	C	O	Fe	Co
Spectrum 1	86.81	12.94	-	0.25
Spectrum 2	88.31	10.42	0.21	1.05
Spectrum 3	89.35	10.32	-	0.34
Spectrum 4	87.41	10.78	0.14	1.67
Max.	89.35	12.94	0.21	1.67
Min.	86.81	10.32	0.00	0.25

A similar study has been conducted by Stopić and Friedrich [14], they focused on polycrystalline diamond blanks with incorporated cobalt (max 1.6% Co). The leaching process using nitric and hydrochloric acid (aqua regia) with ultrasound is optimized at temperatures between 60°C and 80°C. The reactor used is shown in Figure 10. Results show accelerated leaching with ultrasound, achieving a desaturated state of PCD with minimal metallic inclusions at low solid-to-liquid ratios 15g/L

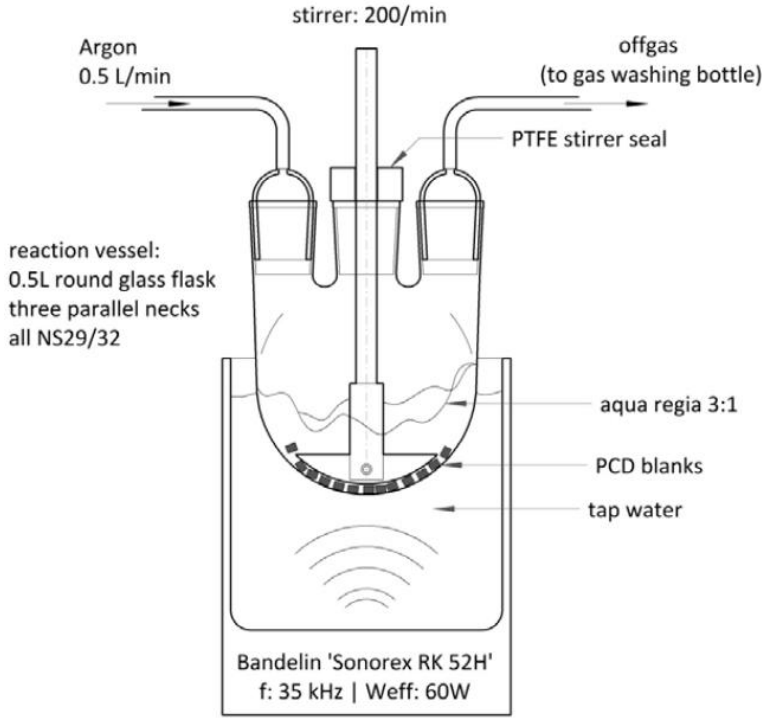

Figure 10: Reaction vessel in an ultrasound bath

1.3 MAGNETIC PROPERTY OF IRON-COBALT

Transition metals can form magnets due to unpaired electrons in their d orbitals. Unpaired electrons create a weak magnetic field, resulting in paramagnetic effects. In coordination compounds, the electron configuration changes due to interactions with ligands, determining whether the compound is paramagnetic or diamagnetic[33].

Ferromagnetism is a physical phenomenon where certain materials, like lodestone (magnetite) and iron, strongly attract others[33, 34]. This means the compound retains its magnetism without relying on an external magnetic field (Figure 11). These natural ferrimagnets were discovered over 2,000 years ago and served as the subjects of early scientific studies on magnetism. Ferromagnetism is a strong magnetism found in iron, cobalt, nickel, some alloys, and rare-earth elements like gadolinium. They are easily magnetized, reach saturation in strong magnetic fields and exhibit hysteresis. Heating beyond the Curie point causes them to lose magnetic properties, but they regain them on cooling [34].

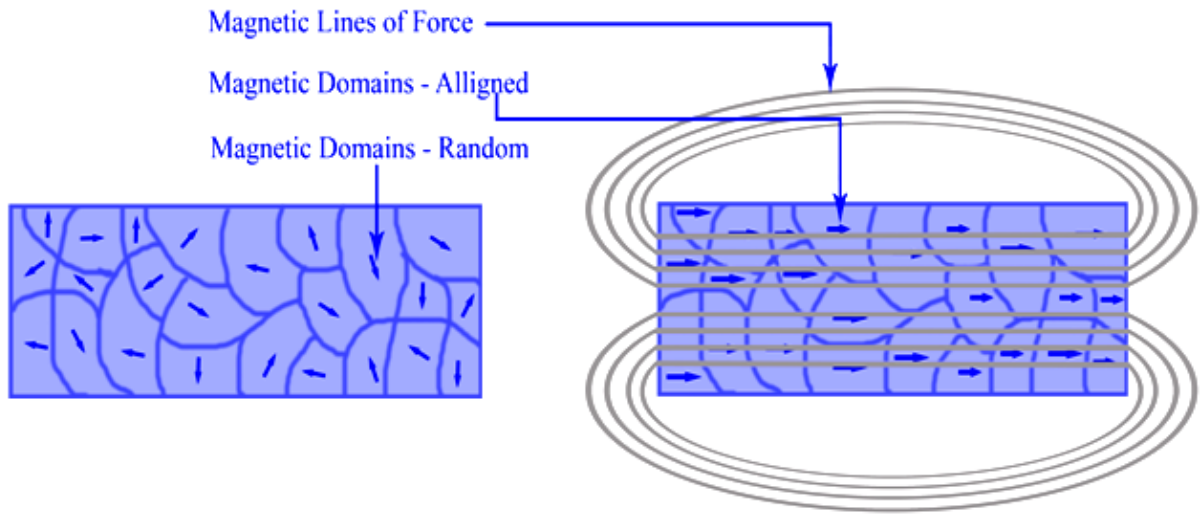

Figure 11: Ferromagnetism (a) unmagnetized material and (2) Magnetized material with corresponding magnetic fields shown [34].

To understand magnetic metals, consider the five types of magnetism:

- Diamagnetism: All matter is weakly repelled by magnets, but in magnetic materials, attraction surpasses repulsion.
- Paramagnetism: Materials weakly attract magnets, like aluminum, oxygen, iron oxide (FeO), and titanium.
- Ferromagnetism: Strongly attracted and can be magnetized, such as iron, cobalt, nickel, some alloys, and rare earth metal compounds. They lose magnetism above the Curie point.
- Ferrimagnetism: Attracted and act as permanent magnets. Lodestones (Fe3O4) are examples, losing external magnetism above the Curie point.
- Antiferromagnetism: Insensitive to magnets at low temperatures, but some atoms break alignment above the Neel temperature, causing weak magnetism. Manganese oxide (MnO) and pure neodymium are examples[35].

1.4 PARTICLES COLLECTION

So far, the methods mostly used for collecting particles include filtration, electrostatic precipitators, and wet scrubber.

Filtration is a method for separating an insoluble solid from a pure liquid or solution. It typically involves using a folded filter paper in a funnel, where the liquid passing through is called the filtrate, and the solid remaining on the paper is the residue[36]. Gravity filtration passes liquid through a porous material, trapping unwanted solids (Figure 12). Filter paper with appropriate porosity and large surface area is best. Glass or plastic funnels can be used, and 'stemless' glass funnels are employed for hot filtration[37]. The key to successful gravity filtration is using fluted filter paper. It reduces contact area with the funnel, allowing rapid filtration. Traditional cone-folded paper slows filtration due to increased contact and thickness, especially during hot recrystallization.

The electrostatic air cleaner is a device that uses an electric charge to remove solid particles or liquid droplets from air or gases (Figure 13). It functions without hindering gas flow and is used for air pollution control, particularly in industrial facilities and power stations. It captures fine particles, which can cause serious health issues and contribute to climate change if released into the atmosphere[38]. Electrostatic precipitators come in various sizes and types for different dust

and gas characteristics. Dry types operate above the gas stream's dew point to remove smoke and dust, while wet types work with saturated airstreams to eliminate liquid droplets in industrial settings, including sticky and combustible particulates.

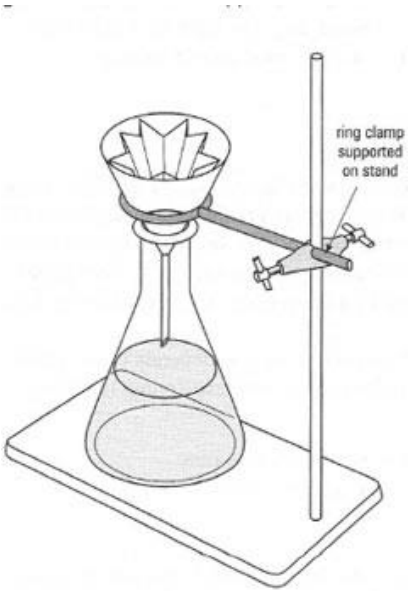

Figure 12: Gravity filtration[38]

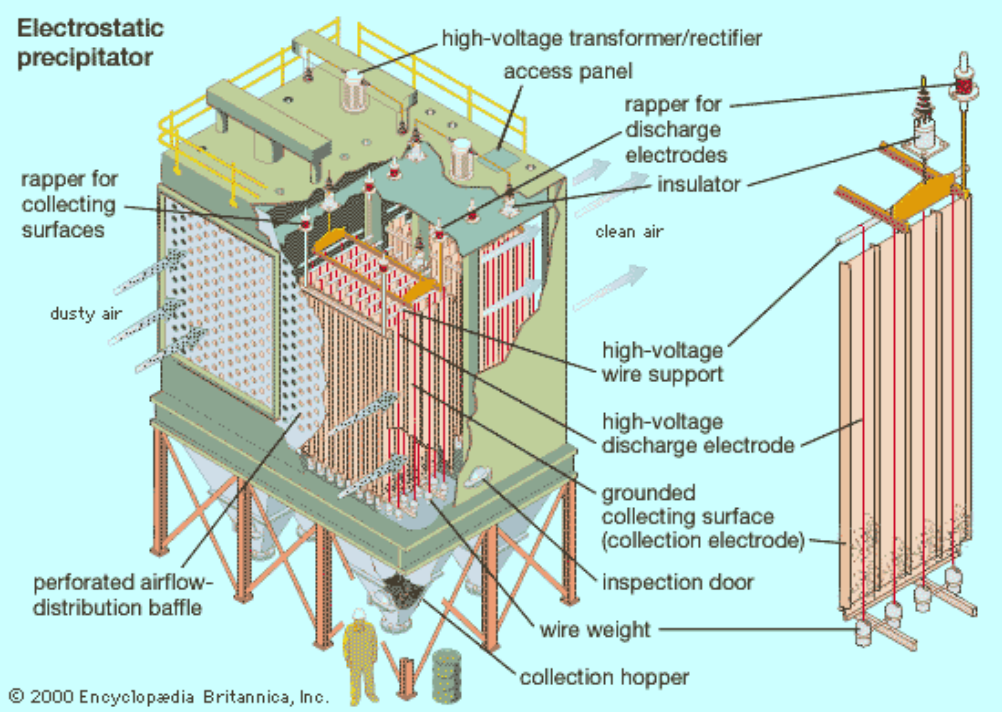

Figure 13: Electrostatic precipitator[38].

1.5 METHODS USED FOR THE SYNTHESIS OF FE-CO POWDER

So far, there are several methods used for the synthesis of Fe-Co powder. The choice of the method depends on various factors such as desired properties of the powders, scale of production, and cost consideration. The common methods are: Chemical reaction, electrodeposition, Spray pyrolysis, Sol-Gel method, Co-precipitation. In the study we used USP and Hydrogen reduction.

1.5.1 Ultrasonic Spray Pyrolysis and Hydrogen reduction

Ultrasonic spray pyrolysis is used to produce ultrafine nanoparticles from a solution or suspension. A USP equipment is composed of three main zones. An ultrasonic spray zone which is connected to the heating zone (tubular furnace) and the collecting zone (bubblers), the ultrasonic spray consists of the aerosol-generating system of a liquid source with an ultrasonic atomizer or ultrasonic nebulizer and the aerosol droplet-carrying system with gas carriers such as (argon, nitrogen, oxygen, hydrogen, etc). The nebulizer consists of a transducer at the bottom of the container in which the precursor solution and the gas are fitted. The gas is used to carry the aerosol to the tubular furnace where thermal decomposition takes place. When an electrical current is applied, the transducer vibrates. The vibration creates capillary waves on the solution's surface in the nebulizer. The atomizing process is misunderstood, but waves passing through the solution and micro cavitation could be the main purpose for the formation of droplets from the bulk solution. These droplets are suspended in the gas phase above the liquid if small enough, aerosol could form. The illustration of a typical USP is shown in Figure 14. The reaction tube is inside the furnace. This oven is connected to a wash bottle where the particles are suspended in deionized water or ethanol to preserve their structure. Particles do not settle directly due to the turbulence caused by the flow of carrier gas into the bottle. The liquid in the first bottle may have trapped some particles. Therefore, two or more bubblers are usually used to collect as much product as possible.

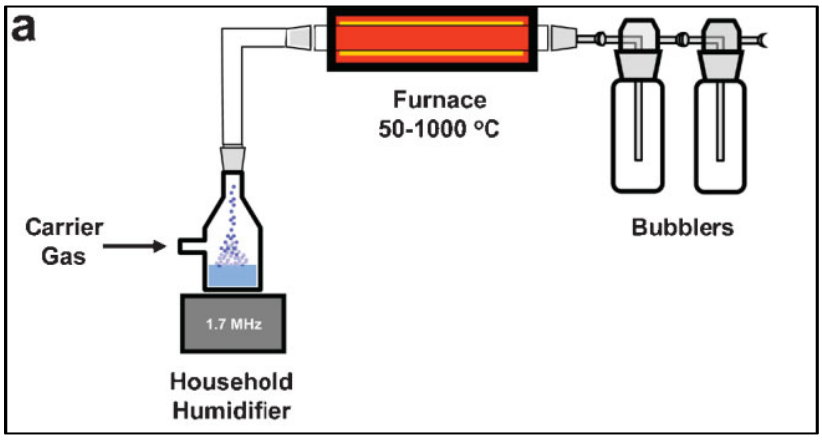

Figure 14: Ultrasonic Spray Pyrolysis process [39]

The aerosol is then carried into a heated chamber by the gas flow, some processes take place in the furnace; here we give a brief description of the process due to the complexity of the entire process. At high temperatures, the solvent evaporates leading to precipitation of the solute, this takes place when the supersaturation point is reached led by the rapid shrinking of the droplet and the heat. The dried particles undergo thermal decomposition to form hollow particles and then go through densification to form solid particles, and Figure 15 shows a simplified USP process. USP can only produce spherical or nearly spherical particles. If not compacted, hollow or porous particles will form. The morphology of the final product depends on the super saturation's degree which is related to two factors: solvent evaporation and the solubility of the starting solution.

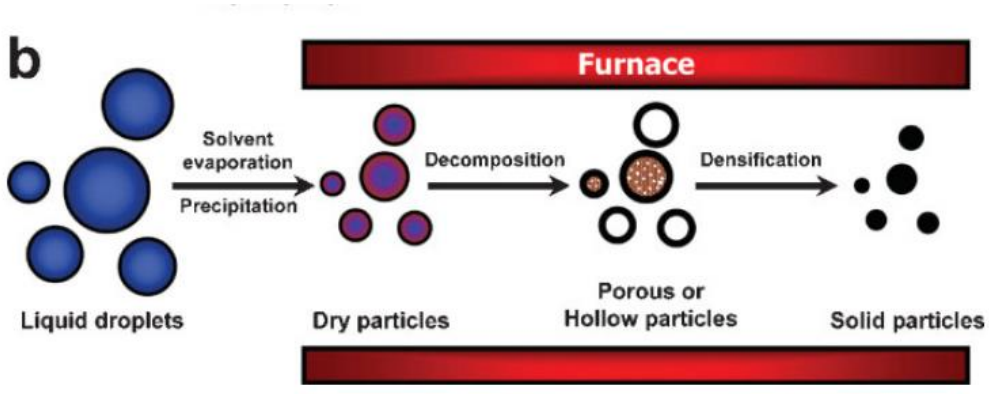

Figure 15: Thermal decomposition process in the furnace [39]

The droplet size is affected by the transducer frequency, the solution density, and the surface tension. Higher frequencies create more turbulence and more microcavities in the solution, which in turn leads to smaller droplets escaping from the bulk solution see Figure 16. The greater the surface tension, the larger the droplets. High density results in smaller droplets, the droplets need to be smaller to be transported by the gas because heavier droplets cannot be suspended in the gas. In a water-based solution, the effect of the surface tension and density is small compared to the frequency effect. The droplet size can be calculated using below Eq1[39], where D is the droplet diameter in cm, γ is the solution surface tension in g/s², f is the frequency in Hz, and ρ is the solution density in g/cm³.

$$D = 0.34\left(\frac{8\pi\gamma}{f^2\rho}\right)^{\frac{1}{3}} \qquad \text{Eq 1}$$

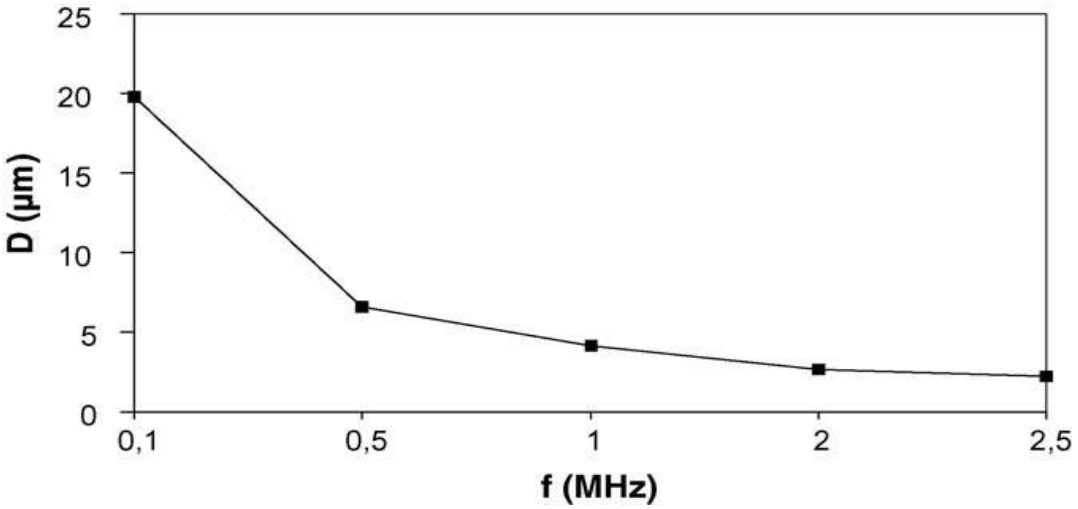

Figure 16: Relation between the droplet diameter and the frequency of the nebulizer*[40]*.

The particle size is determined by the droplet, it is derived from the droplet size by taking to account the evaporation of the solvent and any reactions that may occur. Particle size depends on droplet size and solution concentration. Assuming no precursor loss during the process, this correlation between concentration and other precursor properties and final particle size can be described by Eq2 which is derived from the equation reported by [40, 41]:

$$D_P = D\left(\frac{c_{salt}M}{M_{Precursor}\rho_P}\right)^{\frac{1}{3}} \qquad \text{Eq 2}$$

where D_P is the particle size, D is the droplet diameter, c_{salt} is the solution concentration, M is the molar mass of the product, $M_{Precursor}$ is the molar mass of the solution, and ρ_P is the density of nanopowders.

The concentration of the solution determines how much mass can settle out of a given drop. This mass will later form particles. To derive the size of the particles from the mass, this mass must be divided by the density of the product. The density of the product is derived from the density of the nanopowder to account for porous structures. In the case of a reaction, e.g. decomposition, taking place during USP, a correction due to the different molar masses of the precursor material and the reaction product must be taken into account.

The physical and chemical processes of USP must take place while the droplets and later the particles are transported through the tube and during the elevated temperatures that allow evaporation, decomposition/reactions, and densification. The time required to pass through the heating zone is called the residence time. It can be calculated using Eq. 3, where t is the time in seconds, V is the volume of the heating zone in dm^3, T_0 is the room temperature in K, q is the flow rate of the carrier gas in L/min and T_r is the temperature in the heating zone in K.

$$t = \left(\frac{V T_0}{q T_r}\right) \qquad \text{Eq3}$$

The selected reaction temperature depends on the decomposition temperature of the precursor components. Concerning gas flow, the temperature profile varies along the length of the reaction tube. The residence time and velocity of the aerosol in the reaction tube also depend on the tube diameter. The gas flow, pipe diameter, and length also determine the velocity and temperature distribution over the pipe cross-section. Tubes with a larger diameter and shorter length exhibit less developed airflow, while longer, smaller-diameter tubes exhibit more developed airflow, as shown in Figure 17 [42]. USP generally does not use spool lengths. However, the aspect of velocity distribution is important in choosing the gas flow, residence time, and temperature parameters that will determine whether the aerosol is completely converted into the desired particles. Figure 18 shows the latest version of USP equipment, PRIZMA; Kragujevac, Serbia

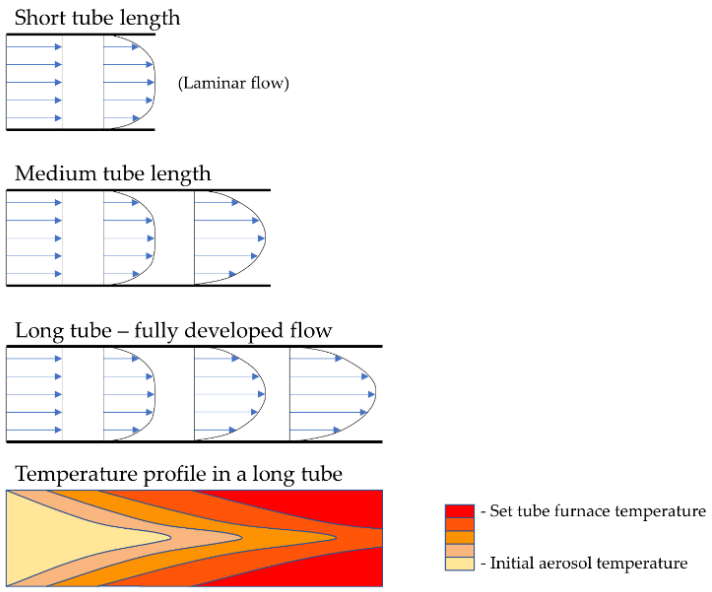

Figure 17: The gas velocity profile depending on temperature, reactor tube diameter, and length[42].

Figure 18: Latest version of USP device (special permission of the company for use in this master thesis)

1.6 E-PH DIAGRAM

The Pourbaix diagram (E-pH) of Iron-Cobalt Nitrate in water solution at room temperature shows the presence of Iron and Cobalt in solid form Co_3O_4, Fe_2O_3, and ionic form Co^{2+}, Fe^{2+}, in the pH area below 2 (acidic system). The figure below shows that with an increased potential between 0.67 and 1.8 V, cobalt is available in the form of ion Co2+ and solid Co3O4, and iron is available only in the form of solid Fe2O3.

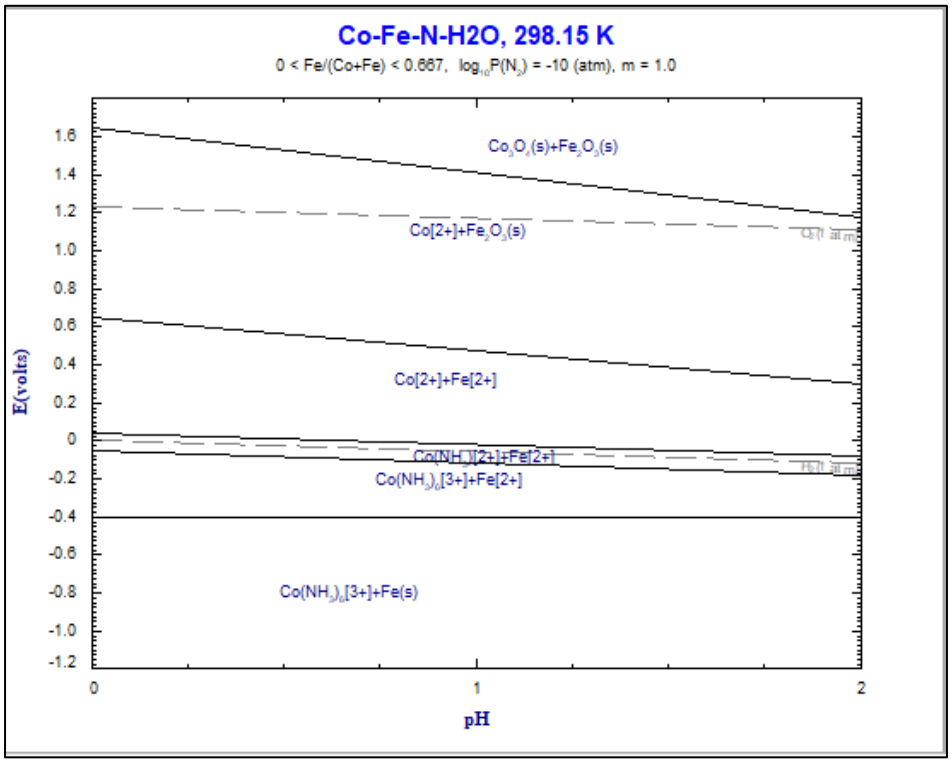

Figure 19: E-pH Diagram

The advantage of USP is the spherical morphology of the particles. The size of these particles can be easily controlled, resulting in a narrow size distribution. Overall, the powder has a relatively uniform composition. Powders with more complex but more compositions that are homogeneous can be easily produced by selecting suitable precursors. It has been reported by Majerič and Rudolf [42] that this method can synthesize nanoparticles from a variety of raw materials, ease to setting up and changing the configuration of individual process sections. The disadvantage is that the residence time during the synthesis is very short, so the process is limited to fast chemical reactions. The overall productivity of the process is low due to the slow rate of aerosol formation from the starting liquid, especially for small droplet sizes. Available plumbing and furnace equipment also

limit the temperature. Therefore, high-temperature synthesis (e.g., carbides, borides, or nitrides) is difficult and based on the effect of smaller particle sizes on reaction kinetics.

1.7 CHARACTERIZATION OF NANOPARTICLES

The synthesized nanoparticles can be characterized by X-ray Diffraction (XRD) to investigate the crystal structure and determine the chemical phase; Scanning Electron Microscopy (SEM) to observe the size and morphology, Energy-Dispersive X-ray spectroscopy (EDX) to analyze the composition of powder, thermal gravimetric analysis, thermodynamic analysis of hydrogen reduction to understanding the fundamental principles governing the metal reduction reaction.

1.7.1 X-ray Diffraction

X-ray diffraction (XRD) is a nondestructive technique for analyzing the structure and composition of crystalline materials[43, 44]. X-ray diffraction employs monochromatic X-rays and a crystalline sample for constructive interference. Produced by a cathode ray tube, these X-rays are filtered for monochromatic radiation, directed at the sample, resulting in diffracted rays. Bragg's Law ($n\lambda=2d \sin \theta$) determines wavelength, diffraction angle, and lattice spacing. Detected and processed, diffracted X-rays provide mineral identification by converting peaks to unique d-spacings compared with reference patterns, achieved by scanning through a range of 2θ angles.[45].

Several researchers have studied crystal structures and chemical phases using XRD equipment. Figure 20 shows the type of results that can be achieved with this device.

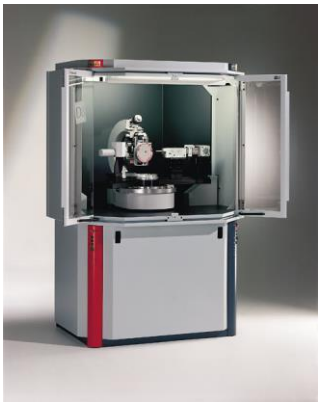

Figure 20: Example of an XRD machine[45].

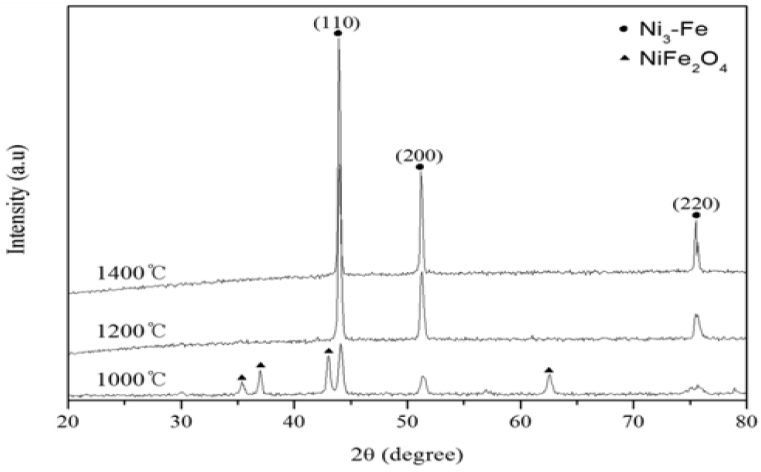

Figure 21: XRD patterns of the powders prepared at various temperatures[46]

1.7.2 SEM/EDS

EDS analysis (Energy Dispersive X-ray Spectroscopy, also known as EDX analysis) is a technique for studying chemical composition on a microscopic scale. Combined with a scanning electron microscope (SEM), EDS obtains compositional information from the X-rays emitted as an electron beam sweeps across a sample. The range of elements that can be detected using this technique covers almost the entire periodic table[47]. The EDS is usually a destructive technique due to cutting the sample to size to fit into the chamber[48]. It is also critical to a range of applications from process/quality control to failure analysis and basic research. Therefore, almost every SEM is equipped with an EDS system[47].

Scanning electron microscopy with energy-dispersive X-ray spectroscopy (SEM/EDS) is an important tool in the field of materials science for studying the structure and composition of a wide variety of samples. It supports advanced surface analysis and can be used in various fields such as product defect investigation and contamination identification[49].

Figure 22 below shows the schema of the SEM/EDS device

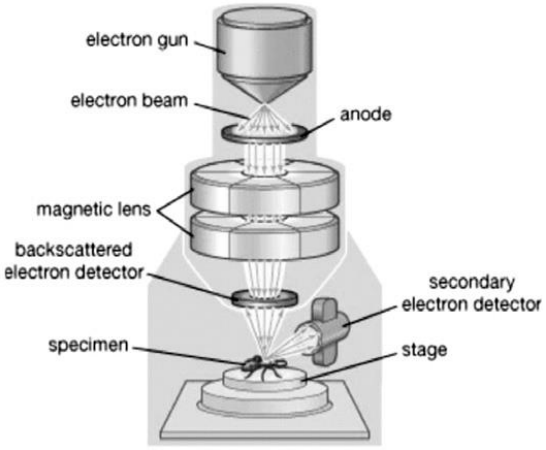

Figure 22: schema of SEM/EDS apparatus

Figure 23 shows the result of the SEM/EDS analysis during this study.

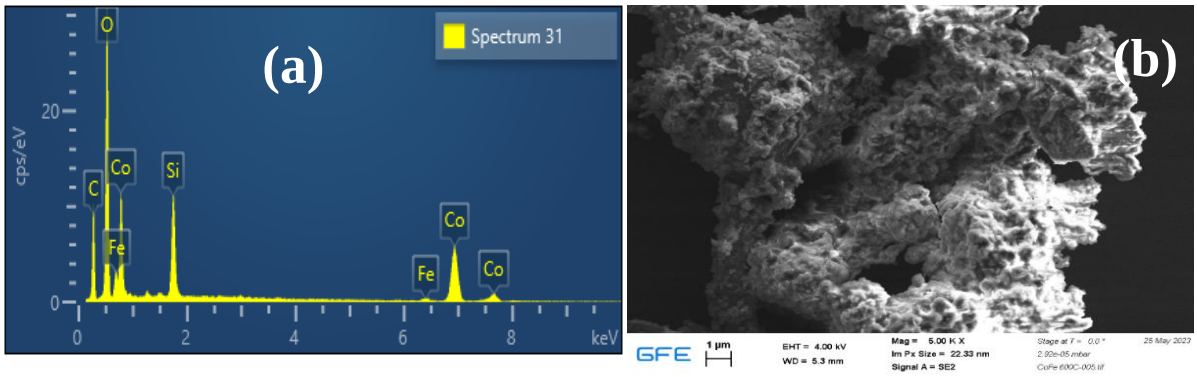

Figure 23: (a) EDS analysis of sample from solution A at 600℃, (b) SEM analysis of sample from solution A at 600℃

1.8 APPLICATION OF NANOPARTICLES OF IRON-COBALT

The nanoparticles have known to be very small size materials and have different properties than the raw materials. They are invisible to the human eye. They show dramatic changes in the chemical composition and physics of larger materials. They are unique due to their mechanical strength, large surface area, and optical and chemical reactivity. Therefore they are involved in many processes such as healthcare, cosmetics, environmental preservation, and air purification[50]. In recent years, these materials have become important players in modern medicine. Clinical applications range from contrast agents in imaging to vehicles for drug and gene

delivery in tumors. In fact, in some cases, nanoparticles enable analysis and therapy that would not be possible otherwise. However, nanoparticles also bring challenges like toxicity[51].

The main applications of iron-cobalt nanoparticles are as follows: magnetic nanoparticles, magnetic data storage and resonance imaging (MRI); in coatings, plastics, nanowires, nanofibers, and textiles, as well as specific alloys and catalyst applications; as raw material, catalysts and pigments[52]. According to [53] magnetic alloy nanoparticles are attractive materials due to their wide-ranging applications in various fields such as biotechnology, medicine, materials science, and engineering. In this context, special attention has been paid to the synthesis of various biomagnetic alloy nanoparticles (BMANPs). The biocompatibility and physical properties of these materials offer great prospects for their application in biomedicine.

Cobalt and cobalt oxide NPs have been widely used in catalysis and biomedicine due to their unique antibacterial, anticancer, catalytic, anti-oxidative, antifungal, and enzyme inhibitory properties[54, 55].

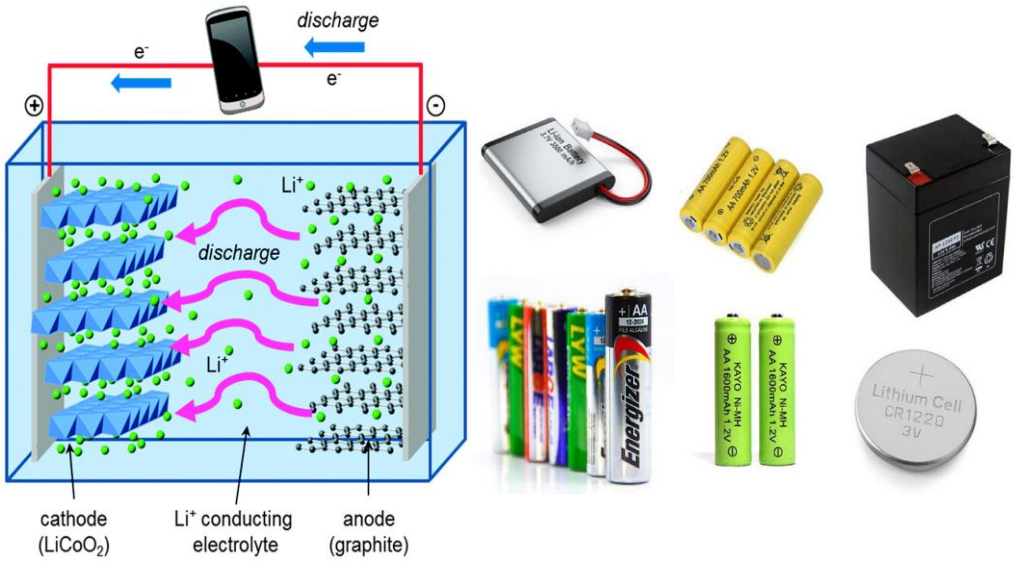

Figure 24: How Li-battery works[56]

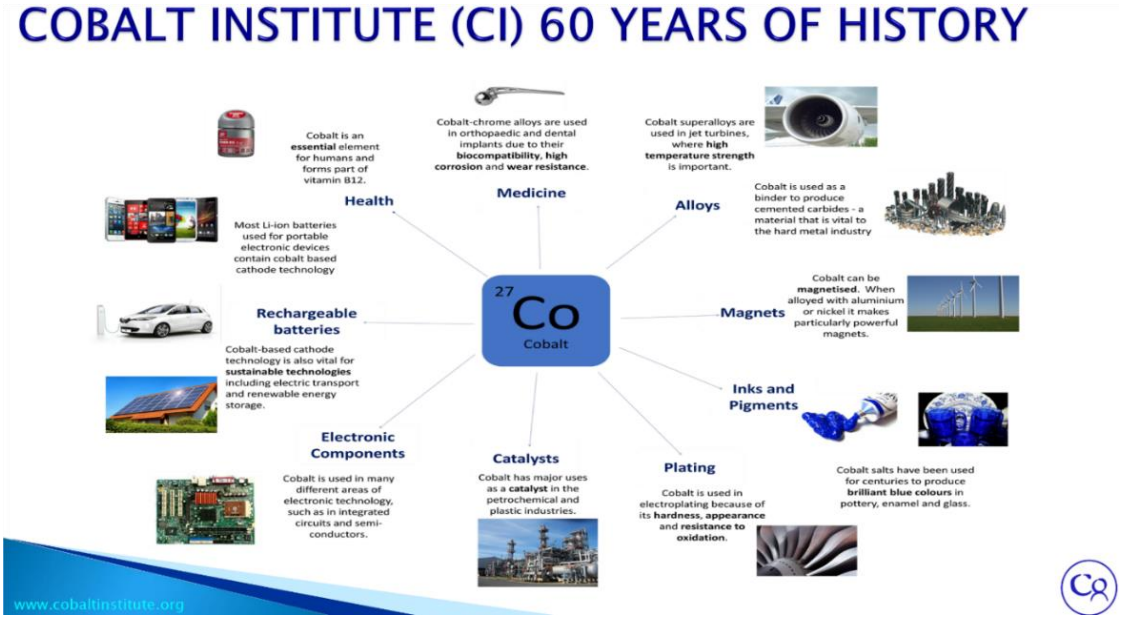

Figure 25: Use of Cobalt*[57]*

PARTIAL CONCLUSION

In this chapter we cover a wide range of topics, from cobalt resources and recovery methods to ultrasonic spray pyrolysis methods, characterization techniques and applications of iron-cobalt alloys. We also discuss their magnetic properties and the importance of efficient powder collection.

Previously, particles accumulated in the wash bottle in the form of a suspension, but this method did not work well as the fine particles were released from the outlet tube. There are currently no data on the use of magnets to collect particles via ultrasonic spray pyrolysis and hydrogen reduction using a secondary cobalt source as feedstock. However, the use of magnets for particle collection represents an innovative and potentially effective system. These findings form the basis of the following chapters, where we explore these topics in more detail and contribute to the growing field of cobalt research.

CHAPTER 2: MATERIALS AND METHODS

Within this chapter, a comprehensive account of the Area study is presented, encompassing meticulous detailing of the methods, tools, and techniques deployed for data collection, data processing, and analysis.

2.1 STUDY AREA

This study is conducted at RWTH-Aachen University, it located in Aachen, Germany, is a renowned German public research university. With over 47,000 students enrolled in 144 study programs, it holds the distinction of being the largest technical university in Germany. The university has been recognized for its excellence, having received funding as a university of excellence for the next seven years through the federal and state excellence strategy. RWTH Aachen has consistently been supported by the DFG (German Research Foundation) and the German Council of Science and Humanities since 2007 as one of the country's top Universities of Excellence. It has also secured substantial third-party funding, ranking first per faculty member and second overall among German universities in a recent survey.

RWTH Aachen University holds membership in various prestigious associations and networks. It is a founding member of CESAER, an association of universities of science and technology in Europe, as well as IDEA League, a strategic alliance of five prominent European universities of technology. Additionally, RWTH Aachen is part of TU9, the association of leading German technical universities. The university is also affiliated with DFG (German Research Foundation).

The Metallurgical Process Engineering Institute, known as IME at RWTH Aachen University (Figure 26), specializes in teaching and research related to metallurgical extraction, recycling, refining, and non-ferrous material synthesis. IME actively engages in applied research and education in areas like extractive metallurgy (covering pyrometallurgy and hydrometallurgy), metal refining, electrolysis, and the recycling of metals from diverse waste sources, in line with circular economy principles. Additionally, IME-RWTH focuses on optimizing resource use, addressing critical waste streams, exploring vacuum metallurgy at various scales, synthesizing nanopowders, and maintains strong ties with the Top Industrial Managers for Europe network,

reinforcing its close connection between academia and industry.

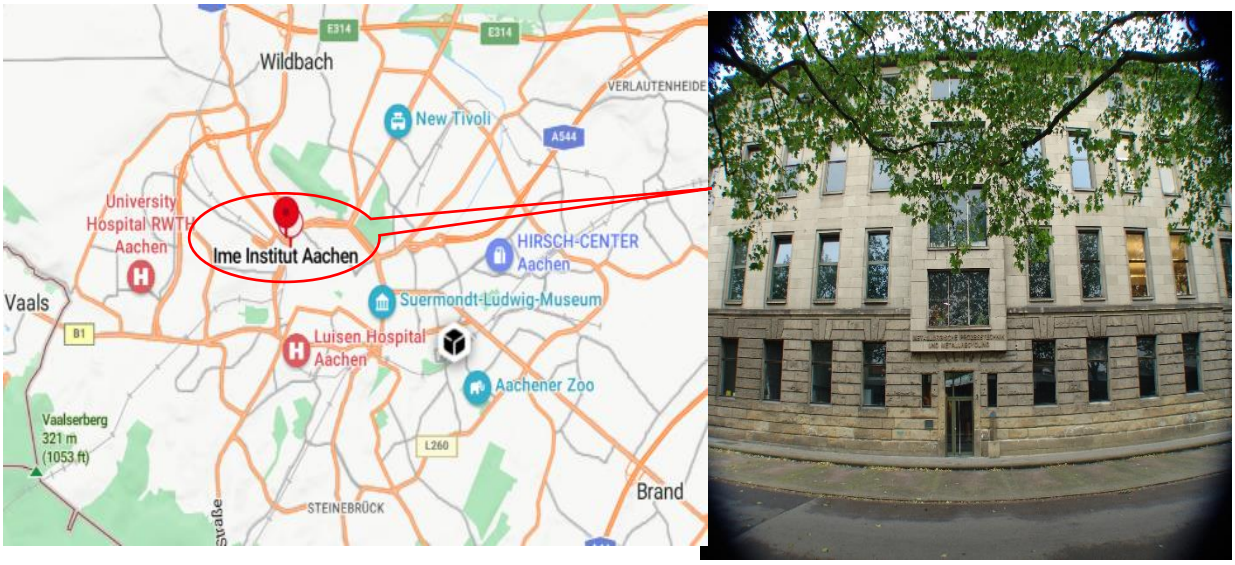

Figure 26: Location of study Area

2.2 PREPARATION OF PRECURSOR

Different precursor was prepared using a solution based on Co and Fe from the leaching of the polycrystalline diamond Blanc with grain size 5 microns of the company REDIES Deutschland without further purification. REDIES produces wire drawing tools made from diamond materials and tungsten carbide. The table 7 and Figure 27 show the concentration of the solutions. The concentration of the original solution was 5.73g/L with 5.63 g/L of Co and 0.1g/L of Fe, the pH was 0.76. We diluted and named the original solution at three levels. Solution A with a concentration of (1.12g/L of Co and 0.02g/L of Fe with a pH), solution B (1.87g/L of Co and 0. 03g/L of Fe), and solution C (2.81g/L of Co and 0.05g/L of Fe). A synthetize solution was prepared with 0.5 mol/l of Co.

Table 7: Concentration of different Solution

SOLUTION	**CONCENTRATION**		**PH**
	Co (g/L)	**Fe (g/L)**	
Original	5.63	0.109	0.7
A	1.12	0.02	1.4
B	1.87	0.03	1.2
C	2.81	0.05	1
Cobalt Nitrate	0.5 mol/L		0.3

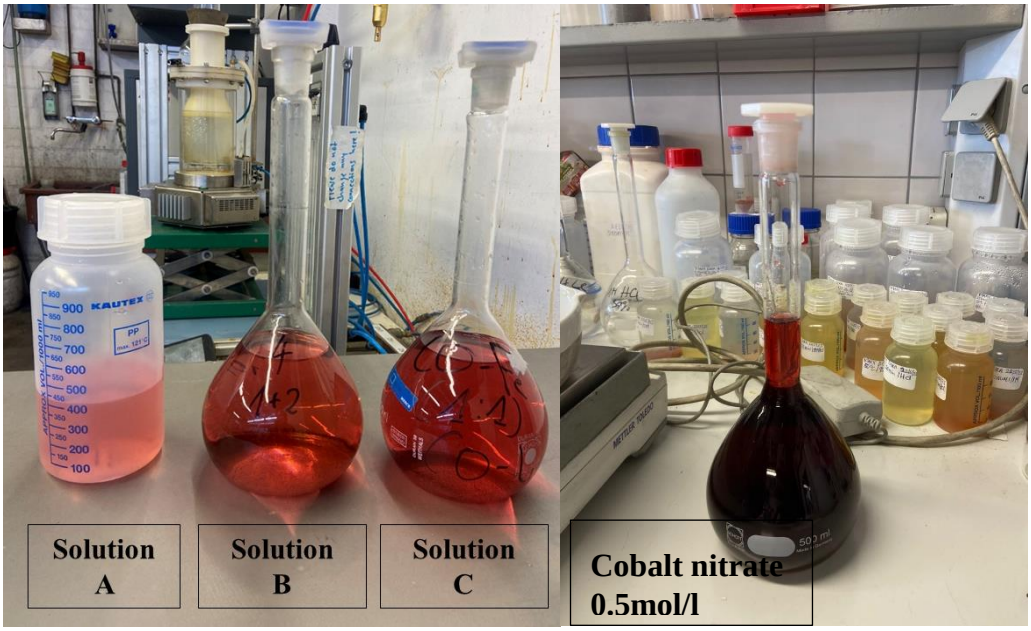

Figure 27: Different solution used.

2.3 EXPERIMENTAL PROCEDURE

Two different types of apparatus were employed in the USP process. The first apparatus, as seen in Figure 28, featured a large furnace (Carbolite furnace model) and an atomizer (Prizma model from Kragujevac), which was used for three sets of experiments. The second apparatus, shown in Figure 30, consisted of two small furnaces (Thermostar) and was used for one set of experiment.

The nanoparticles of Co-Fe were prepared by ultrasonic spray pyrolysis method. The basic concept consists of an aerosol-generating system connected to the heating zone in which the aerosol is pyrolyzed in the pre-heated chamber and a washing zone for collecting particles product.

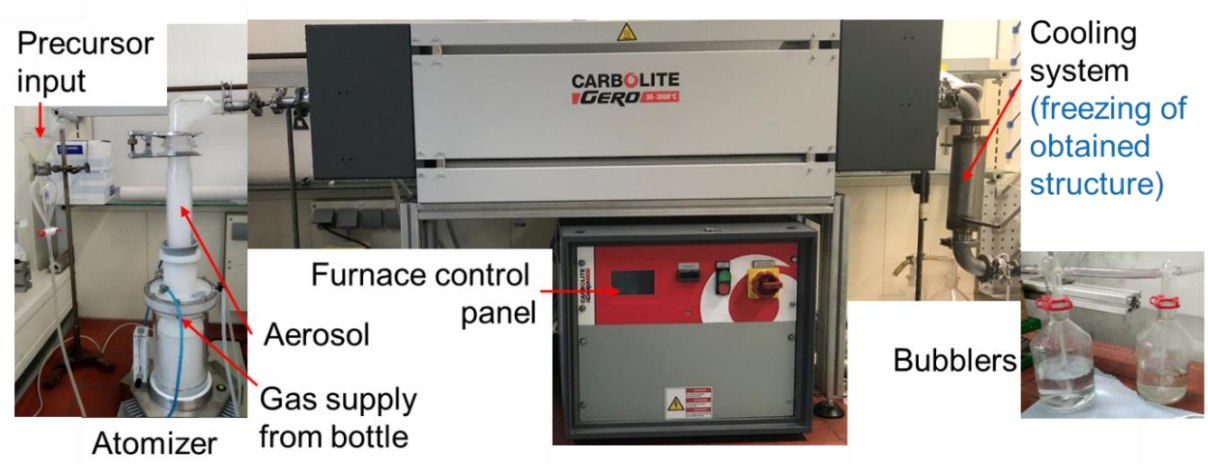

Figure 28: Schema of Carbolite furnace

The three first set of experiment was performed using a Carbolite furnace (large furnace). The transition from droplets to particles takes place in a quartz tube with a length of 95 cm, and 40 mm as inside diameter. The atomizer (model Prizma, Kragujevac, at 1.75 MHz as frequency) uses three piezoelectric crystals connected to a frequency generator (70 percent of the total power has been used). The precursor solution was introduced through a funnel connected to a hose at the bottom of the nebulizer. This allows repopulation later in the test run. So the process can continue indefinitely as long as enough precursors are made. A carrier gas is introduced over the precursor solution, which determines the maximum liquid level and thus the volume that can be filled initially. Argon or a mixture of argon and hydrogen was used as the carrier gas. Adjust the gas flow rate with a rotameter and mix at the outlet of the rotameter. Hydrogen is used as a reducing agent.

The duration of the experiment is limited by the time required to bring the furnace up to temperature, depending on the heating rate. The large furnace has a programmed rate of 400°C/hr and the small furnace has a rate of approximately 300°C/hr. The large furnace also cools more slowly and is only safe to shut down at temperatures of 500 °C. This extends the overall duration of the experiment to longer than the hold time in which the reaction occurs. Therefore, the maximum hold time must be tied to working hours and access to the device.

The residence time of the large furnace is shown in Figure 29. At room temperature the residence time will be up to 23 seconds at 3 l/min, the shortest residence time is 7.19 seconds it has been observed at 900 ℃ at 3l/min as flow rate. To prolong the residence time, the gas flow is therefore

limited to the minimum that still ensures aerosol flow into the reaction tube.

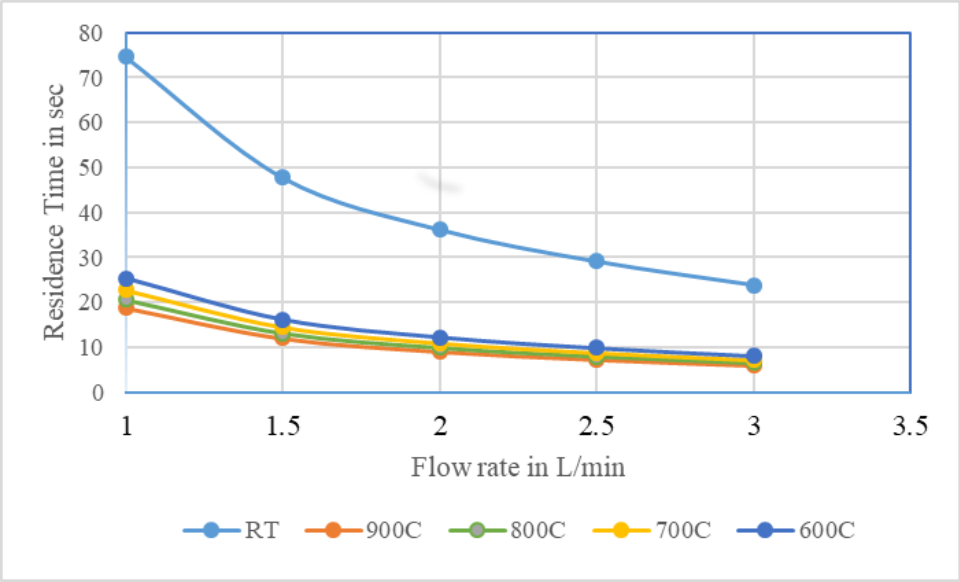

Figure 29: Residence Time for Carbolite furnace Setup

A series of experiments was conducted utilizing two thermostatic furnaces positioned adjacent to each other. In these experiments, particles were generated using solution A as the precursor at different temperatures ranging from 600 to 900°C. This particular furnace configuration was selected due to its short residence time seen in Figure 30, which is advantageous for the experiment. The furnace consists of three main components, similar to the large furnace.

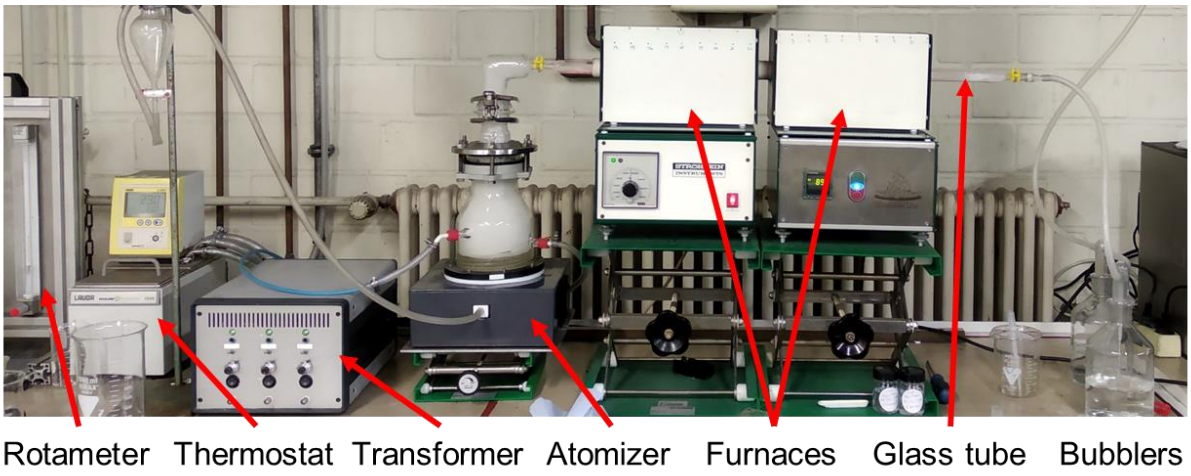

Figure 30: Thermostar set-up

Figure 31 illustrates the residence time of the small furnace. At room temperature, the residence time can reach up to 7.19 seconds when the gas flow is set at 3 l/min. The shortest residence time of 1.81 seconds was observed at a temperature of 900°C with a gas flow rate of 3 l/min.

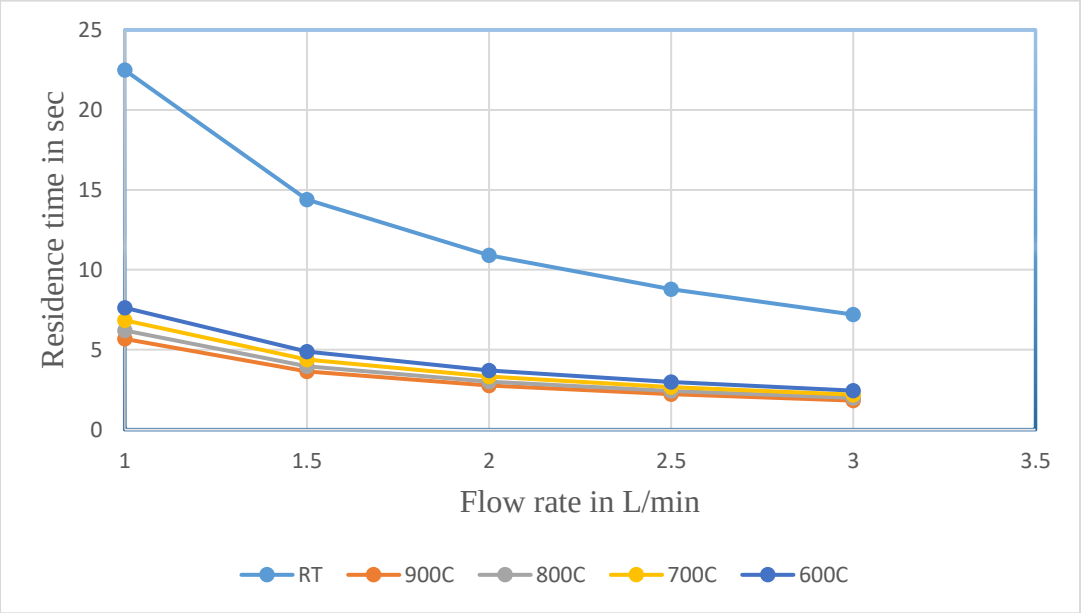

Figure 31: Residence time for Thermostar set up

2.4 COLLECTION OF PARTICLES

Two methods were employed to collect particles. The first method involved gathering particles from the glass bottle, while the second method utilized a magnet.

For the first method, the collection of particles occurred in two steps. Initially, the particles generated from the USP process were collected using a glass beaker measuring cup (as depicted in Figure 32, without requiring measurement). Subsequently, the particles were allowed to settle at the bottom of the glass beaker. In the second step, a vacuum pump, illustrated in Figure 33 (Model Ilmvac LVS610 Tp), was utilized to separate the liquid from the particles.

Figure 32: Generated particles from USP in a glass beaker.

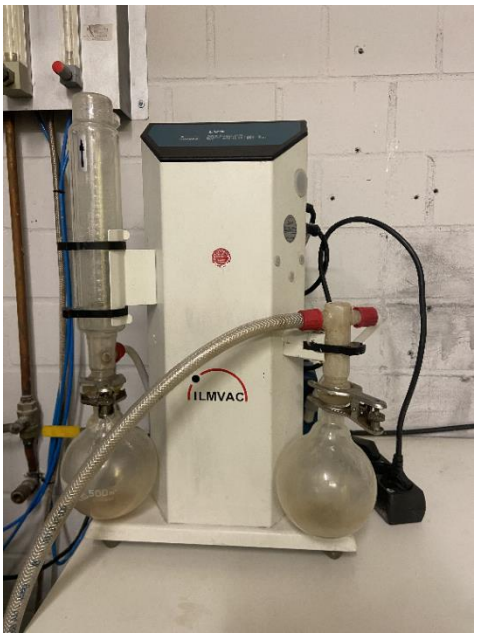

Figure 33: Vacuum Pump

The second method involved the use of magnets, as depicted in Figure 34, to collect particles both in the tube after exiting the furnace and in the glass bottle.

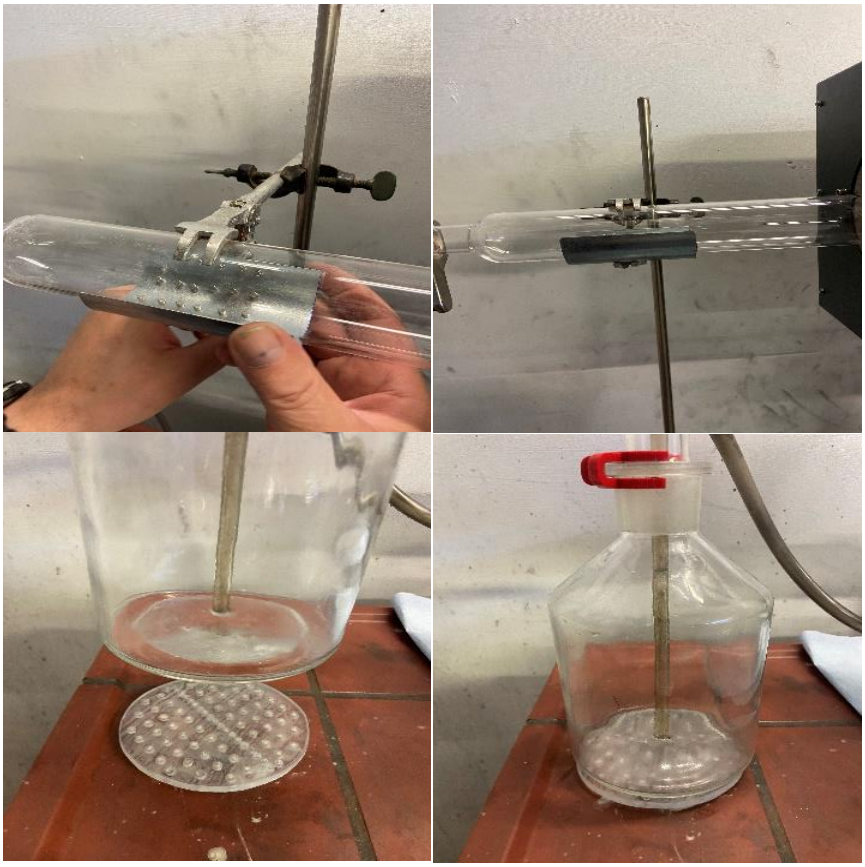

Figure 34: Illustration of the two different magnet system for particle collection (in cooperation with REDIES Deutschland GmbH)

2.5 PREPARATION OF SAMPLE

The sample was prepared by removing the liquid from the particles and placing them in a small transparent glass container (as shown in Figure 35). This container was subsequently placed in a dryer shown in Figure 32 (Thermo Scientific Heraeus).

Figure 35: Sample in the transparent glass container

Despite the efforts of the vacuum pump, the liquid could not be completely removed, resulting in the particles still being wet. Therefore, a drying process was necessary to ensure that the sample was ready for various analysis.

Figure 36: Dryer (Thermo-Scientific)

2.6 DATA ANALYSIS

Many analysis methods were used to characterize the sample. X-ray Diffraction (XRD) was used to investigate the crystal structure and determine the chemical phase; Scanning Electron Microscopy (SEM) was used to observe the size and morphology, Energy-Dispersive X-ray spectroscopy (EDX) was used to analyze the composition of powder, and the software FactSage was used for thermochemical analysis.

IPCOES (Inductively Coupled Plasma Optical Emission Spectrometry) also called Inductively Coupled Plasma Atomic Emission Spectroscopy is an analytical technique used for the detection of chemical elements, it has been used to analyze the original solution before the experiment.

2.7 PARAMETERS

The experimental parameters are specified in detail in table 8 and table 9. The large furnace conducted 16 experiments, as indicated in table 8, while the small furnace performed 4 experiments, as presented in table 9.

Table 8:Parameters used for the large furnace

EXP. RUN	SOLUTION CONCENTRATION (G/L)	FLOW RATE (L/MIN)	TEMPERATURE (°C)	REACTION TIME (H)
1	A	3	600	2
2	A	3	700	2
3	A	3	800	2
4	A	3	900	2
5	B	3	600	2
6	B	3	700	2
7	B	3	800	2
8	B	3	900	2
9	C	3	600	2
10	C	3	700	2

11	C	3	800	2
12	C	3	900	2
13	C	3	700	2
14	C	3	800	2
15	C	3	950	2
16	Cobalt nitrate (mol/L)	3	950	2

Table 9:Parameters used for the small furnace

Exp. Run	Solution Concentration g/L	Flow rate L/min	Temperature °C	Reaction time (h)
1	A	3	600	2
2	A	3	700	2
3	A	3	800	2
4	A	3	900	2

PARTIAL CONCLUSION

In this chapter, we carefully outline the materials and methods used in the study and establish the framework on which analyzes and results are based. Through selection of analytical techniques such as SEM, EDS, and XRD, we characterized the particles under study. Furthermore, our systematic study of key parameters such as temperature, concentration, residence time and particle collection method provides a solid foundation for the upcoming results chapter. As we begin to examine our findings in detail in the next chapter, the understanding of the experimental design and procedures described here will be critical for the reader to understand the context of our results.

CHAPTER 3: RESULTS AND DISCUSSION

This chapter encapsulates the outcomes of diverse analyses, such as SEM, EDS, and XRD, and examines the effects of various parameters, including temperature, concentration, and residence time, as well as different collection methods.

3.1 RESULTS

3.1.1 Influence of temperature on Fe-Co particles synthesis

3.1.1.1 Using Energy Dispersive Spectroscopy (EDS) analysis

The reaction temperature has a significant effect on the specific surface area, surface morphology, nucleation, and growth of powder particles. Through EDS analysis, the influence of the temperature from 600°C to 900°C on the chemical composition of the solution A sample is shown in Table 10. The atomic percentage of Co increases with increasing temperature, and the atomic percentage of Fe decreases with increasing temperature. This means that the elevated temperature is suitable for the extraction of cobalt. The table shows that the atomic percent of oxygen decreases slightly with increasing temperature. This increase may be suitable for removing some traces of oxygen, thereby increasing the rate of hydrogen reduction. Silicon and aluminum appear to be temperature resistant; however, Al exhibits a disproportionate change.

In the study of Choa et al. [58], metal/ceramic nanoporous nanocomposite powders were prepared and characterized using ultrasonic spray pyrolysis. The initial material was derived from Fe and Mg nitrates dissolved in pure water. A mist was formed and directed into a preheated chamber (500-800°C) by an air carrier gas. The results demonstrated that increasing the chamber and reduction temperatures led to larger particle sizes in the Fe/MgO samples. Shatrova et al. [59] Investigated on Elaboration, characterization and magnetic properties of cobalt nanoparticles synthesized by ultrasonic spray pyrolysis followed by hydrogen reduction. They found that the effective diameter of the samples varied with pyrolysis temperature, increasing from 55 to 270 nm as temperature rose, except for the 700°C sample, which had larger particles. Similarly, for samples at different reduction temperatures, the average nanoparticle size followed a consistent trend, growing from 85 to 198 nm with increasing temperature.

Table 10: EDS anlysis result of Fe-Co particles from solution A at different temperatures (600-900 °C)

Temperature (°C)	Element (at.%)				
	Co	**O**	**Fe**	**Si**	**Al**
600	28.58	55.65	1.94	13.84	-
700	30.48	53.77	1.27	11.67	1.95
800	32.94	40.86	3.28	15.34	10.33
900	29.02	54.23	0.86	13.98	1.58

The spectral patterns exhibited consistent features, with prominent peaks for carbon, oxygen, cobalt, and silicon (Figure 37). Surprisingly, the silicon peak was noticeable and exhibited a gradual decline with rising temperature, possibly due to interactions with the ceramic tubes in the furnace. Conversely, the iron peak was smaller, in line with expectations.

Unexpectedly, the presence of aluminum, titanium, and chlorine peaks was detected, suggesting that these elements should not have been present in the sample. In contrast, the spectrum clearly indicated substantial quantities of oxygen, cobalt, carbon, and silicon, all of which were easily identifiable, while iron appeared to be present only in trace amounts. These findings shed light on the element composition and behavior of the particles under varying temperatures.

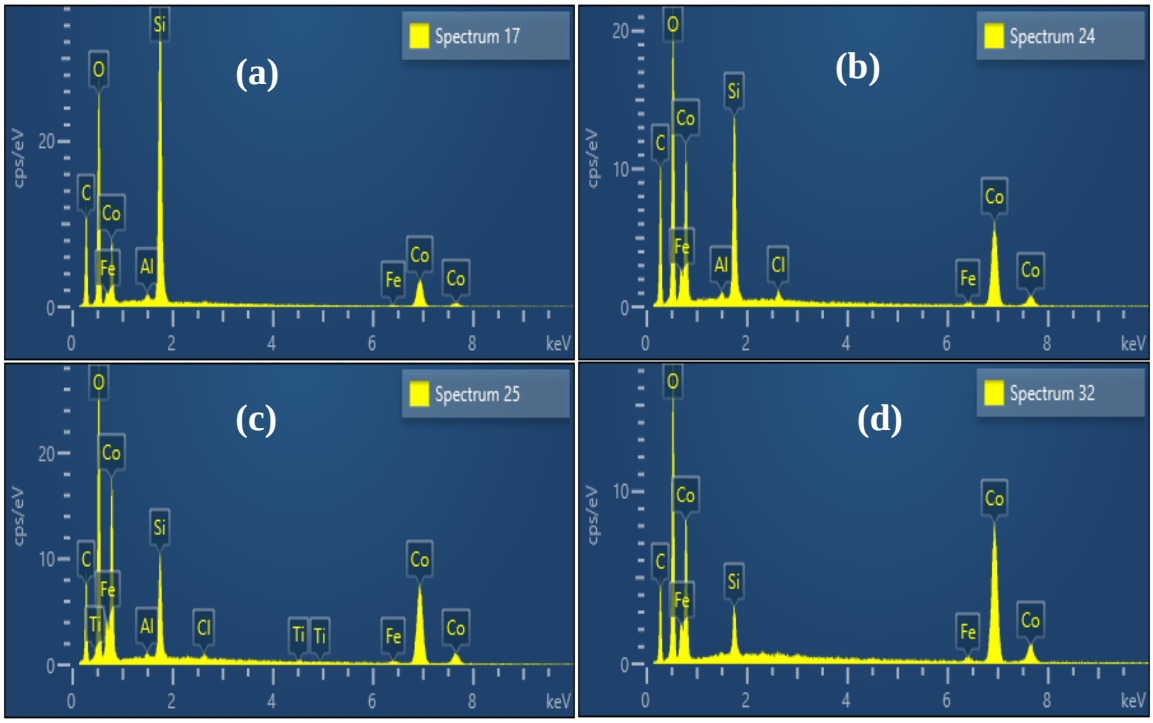

Figure 37: EDS analysis of solution B at 600ºC (a), 700ºC (b), 800ºC (c), 900ºC (d)

Figure 38 illustrates the findings, revealing that fluctuations in precursor concentration do not significantly impact the elemental composition of the samples. Throughout the temperature range, the elemental composition remains relatively constant, with the presence of carbon (C), oxygen (O), silicon (Si), cobalt (Co), and iron (Fe). Furthermore, traces of sodium were observed at 600 °C, 700 °C, and 900 °C, while traces of aluminum and chlorine were detected at 700 °C and 900 °C. These results provide valuable insights into the stability and consistency of the elemental constituents within solution C under different thermal conditions.

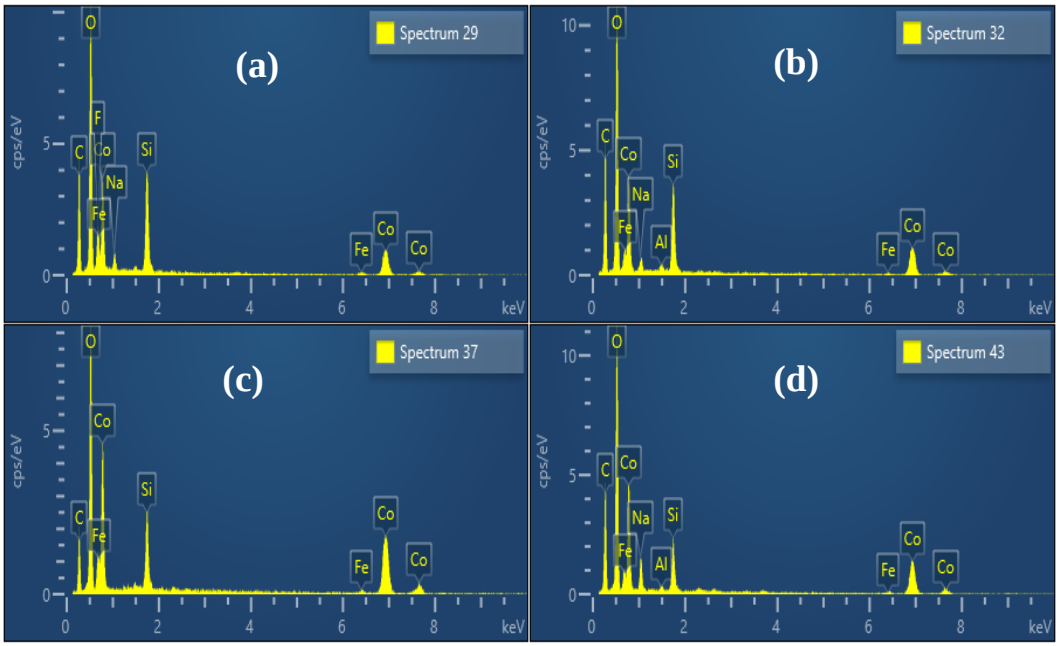

Figure 38: EDS analysis of solution C at 600ºC (a), 700ºC (b), 800ºC (c), 900ºC (d)

3.1.1.2 Using Scanning electron microscopy (SEM) analysis

Figure 39 displays SEM results of Fe-Co samples in Solution A at different temperatures, showing diverse nanoparticles. As temperature rises, agglomerated Fe-Co particles with varied crystal planes form. Notably, solid particles are seen between 600°C and 800°C. Figure 40 reveals SEM images of Solution B's sample, exhibiting changing particle distributions with temperature. Figure 41 presents SEM results of Solution C's sample, featuring assorted nanoparticles with agglomerated spherical Fe-Co particles and crystal facets, forming sphere-shaped agglomerates.

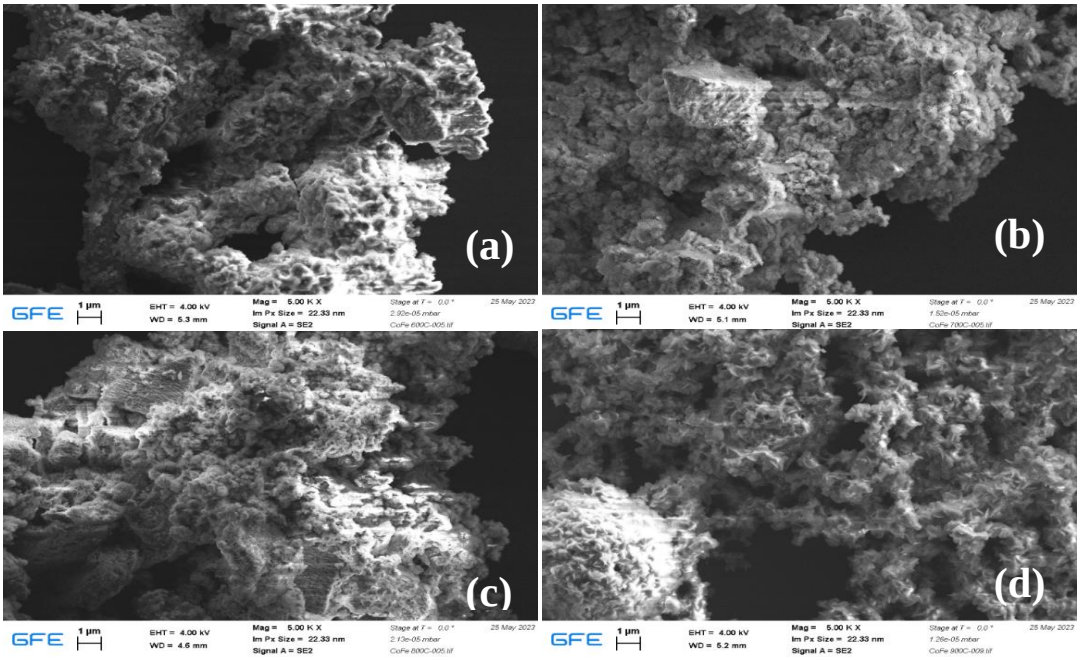

Figure 39: SEM analysis of particles from solution A at 600ºC (a), 700ºC (b), 800ºC (c), 900ºC (d)

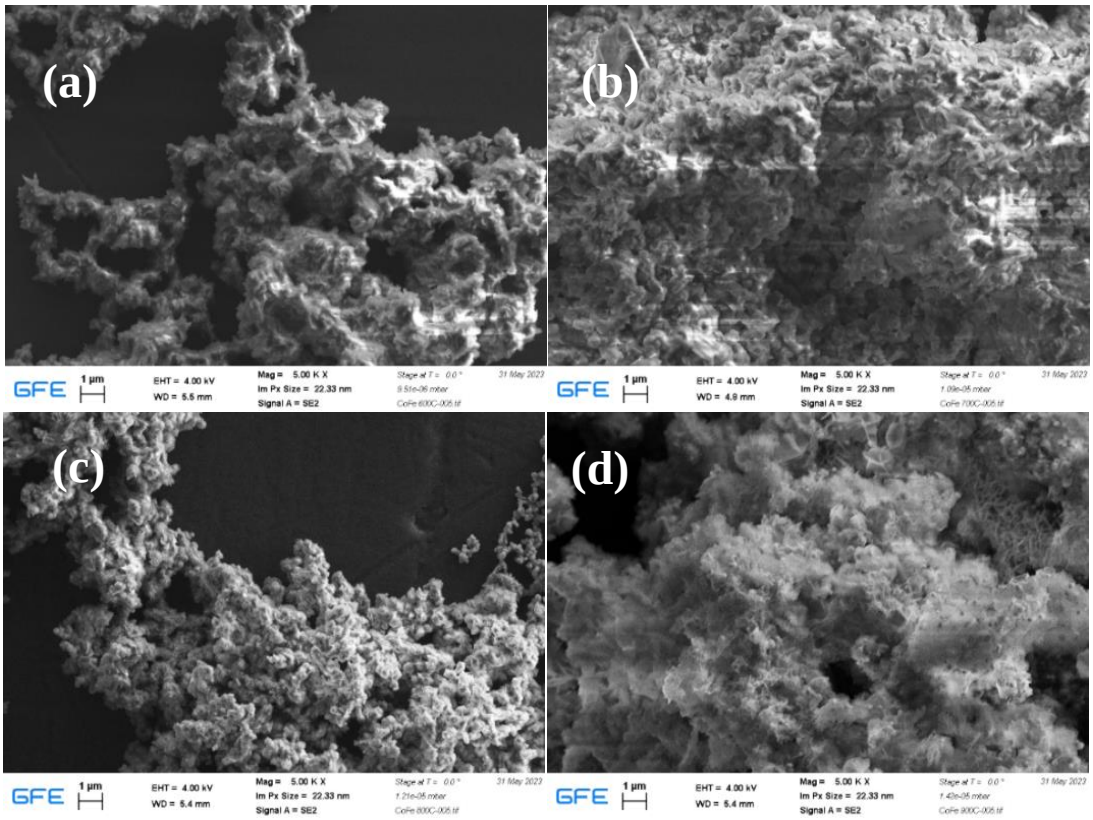

Figure 40: SEM analysis of particles from solution B at 600ºC (a), 700ºC (b), 800ºC (c), 900ºC (d)

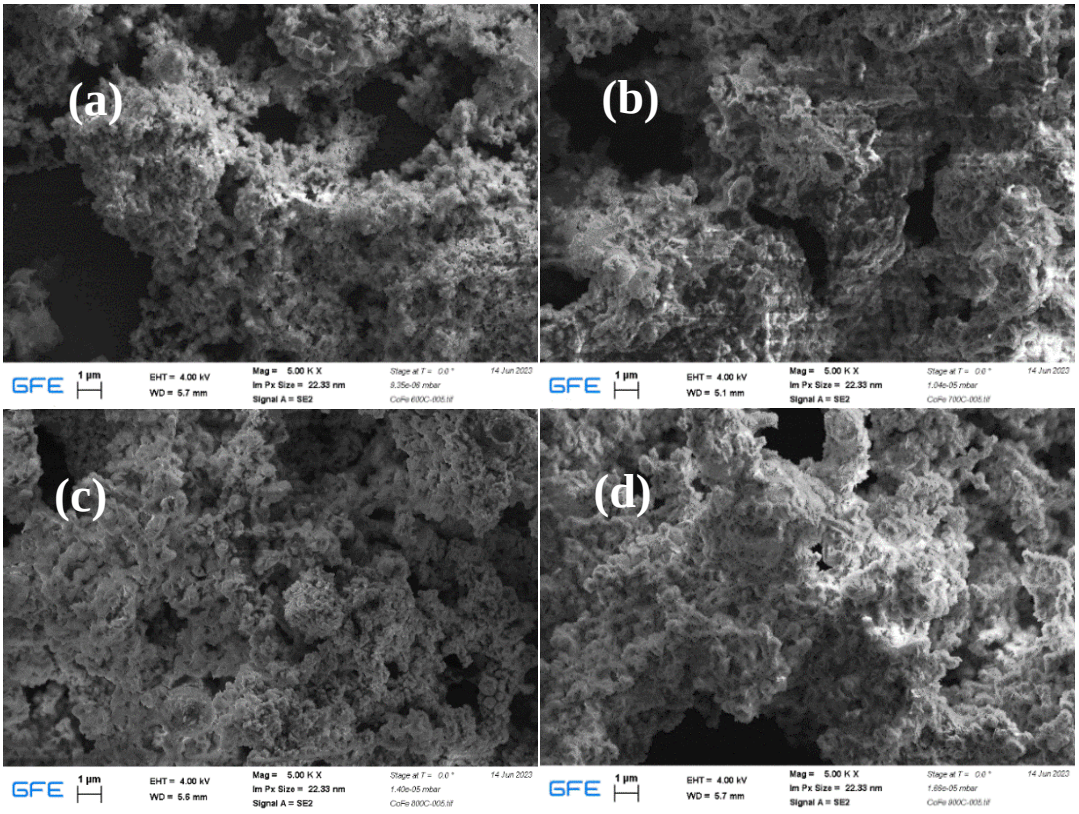

Figure 41: SEM analysis of particles from solution C at 600ºC (a), 700ºC (b), 800ºC (c), 900ºC (d)

3.1.2 Influence of the concentration of precursors

This study examines the influence of different precursor concentrations on the particles obtained, utilizing Ultrasonic Spray Pyrolysis (USP) and hydrogen reduction. The experiments were conducted with a 2-hour run time, reduction temperatures ranging from 600°C to 900°C, and a precursor containing Co and Fe extracted from leaching the polycrystalline diamond Blanc with a grain size of 5 microns. The reduction process involved a volumetric flow rate of 2 l/min H2 and 1 l/min Ar.

Figure 42 shows the SEM result of different precursor concentrations at 900ºC. As the concentration of cobalt increases, the sample shows higher crystallinity and a morphological change from rod-like shapes. In Figure 37(a) the agglomeration is more pronounced, no spherical particles. Figure 37(b) shows some agglomerated and spherical particles. In Figure 37(c) some small spherical particles are formed. The increase of the concentration of cobalt in the precursor drive to the increase of particles size, we can confirm that it has an impact on the distribution size

and the morphology of particles. In the investigation conducted by Gürmen et al. [40], the impact of precursor concentration was studied within the range of 0.04–0.08 M, while maintaining conditions of a 2-hour run time, an 800°C reduction temperature, and a volumetric flow rate of 1 l/min H2. The findings from this study confirmed that reducing the concentration of cobalt nitrate led to a decrease in particle size. A similar investigation has been made by Stopić et al. [41] and Gurmen et al. [60] Conducted the synthesis of silica powder by subjecting a highly concentrated colloidal solution (30%) to ultrasonic spray pyrolysis at a temperature of 900 °C. The investigation verifies that reducing the concentration from 0.5 to 0.125 mol/L results in a decline in the measured average diameter, diminishing from 690 to 610 nm.

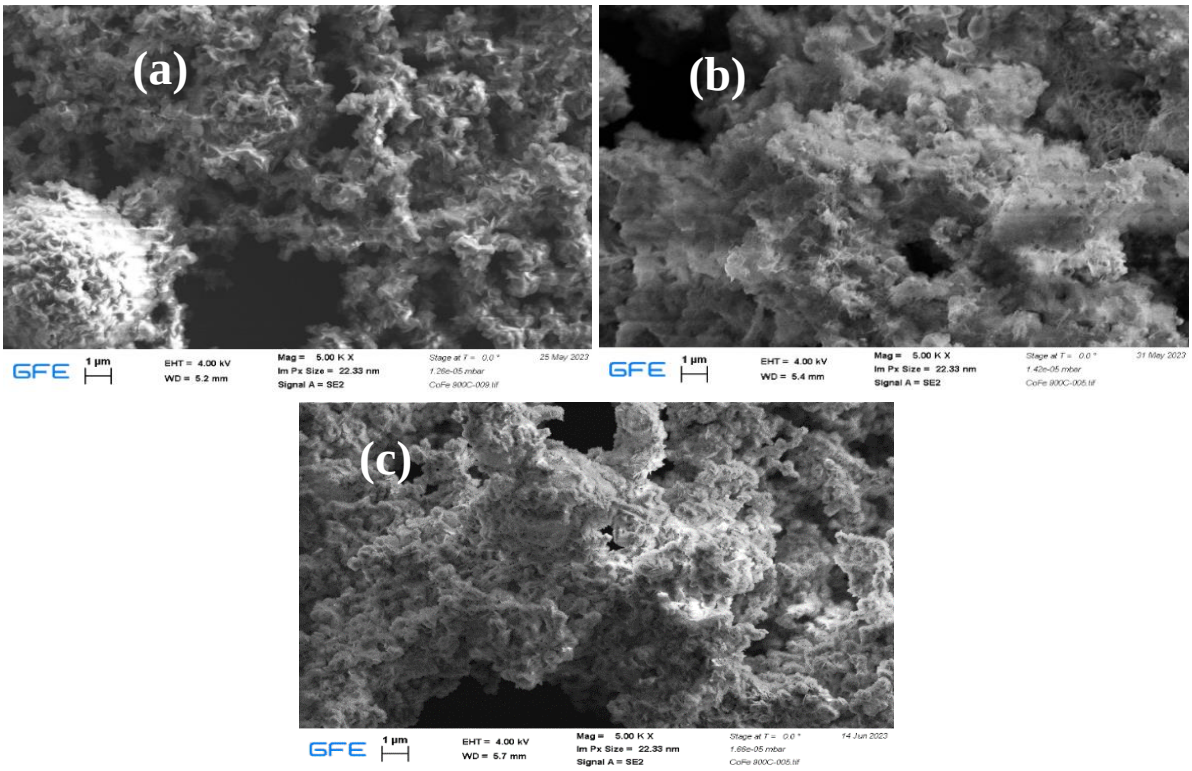

Figure 42: SEM of Fe-Co nanoparticle at 900^{o}C with different concentrations of precursors (a) solution A, (b) solution B, (c) solution C

3.1.3 Influence of the residence time on the particles

The impact of the residence time on the particles obtained by ultrasonic spray pyrolysis and hydrogen reduction of the solution A at 600^{o}C and 900^{o}C is shown in Figure 43 and Figure 44.

Two different residence times were used 23 seconds for the larger furnace and 7.19 seconds for the small furnace at room temperature with a gas flow rate of 3l/min.

SEM reveals the presence of spherical particles with the range of 191.1nm – 1222nm using the residence time of 7.19 seconds as shown in Figure 43(a). In Figure 43(b) the agglomeration is more pronounced using the residence time of 23 seconds. From the SEM results, we can assume that the short residence is more favorable for the nanoparticle synthesis of Cobalt. On the other side, we expect that higher residence time leads to a complete reduction of cobalt nitrate to cobalt using hydrogen. In EDS analysis, Figure 44(a) demonstrates a prominent cobalt peak at short residence time, whereas Figure 44(b) depicts a smaller cobalt peak at longer residence time.

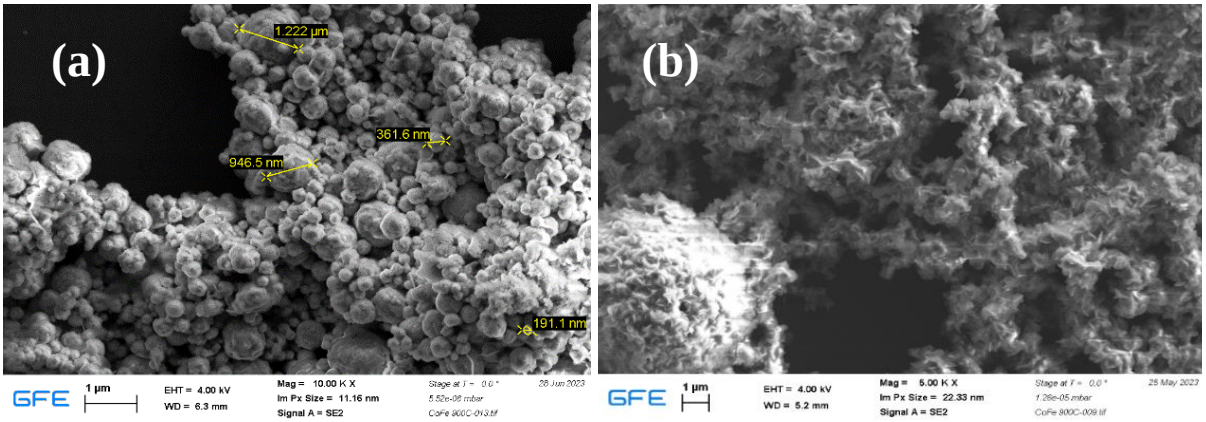

Figure 43: SEM analysis result of Fe-Co nanoparticle at 900^{o}C at different residence time

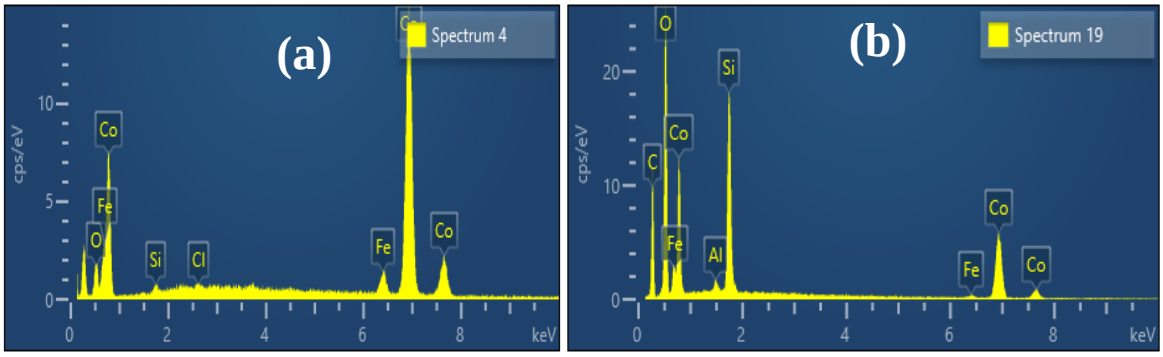

Figure 44: EDS analysis result of sample from solution A using short residence time (a) and high residence time (b)

3.1.4 Magnet collection of particle

The EDS analysis results of the sample from solution c collected using a magnet are presented in Figure 45(a) and Figure 45(b). The findings indicate the presence of numerous inspected particles displaying both high and low peaks. Notably, the target elements, iron, and cobalt, are observable.

Additionally, the SEM analysis results are shown in Figure 45(c) and Figure 45(d). These results demonstrate an irregular distribution of small particles. Figure 45(c) depicts solid particles and small nanoparticles with sphere shapes, while Figure 45(d) reveals small particles exhibiting a sphere shape as well.

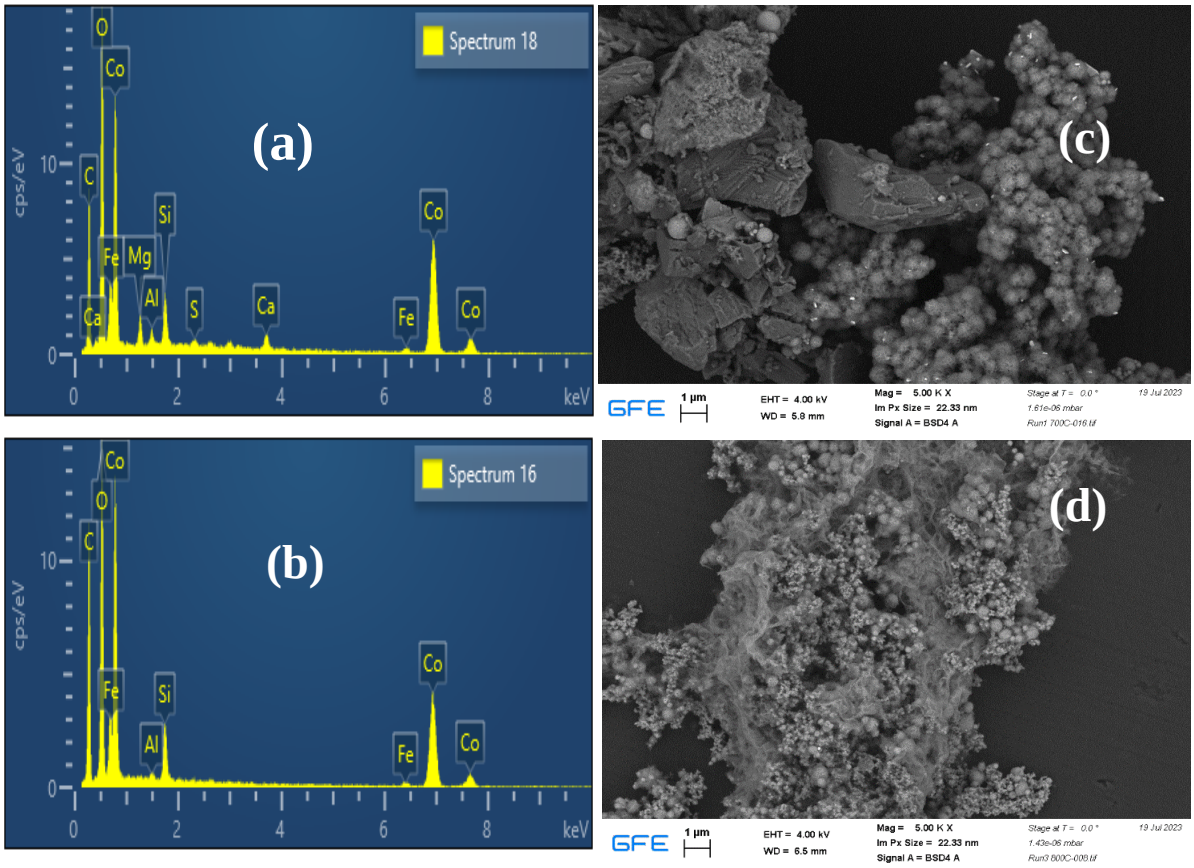

Figure 45: SEM/EDS analysis of particles from solution C at 700°C (a-c), and at 800°C (b-d) using a magnet in the collecting system

Magnetic testing was conducted on the obtained particles using a small magnet (Figure 46), confirming their magnetic nature.

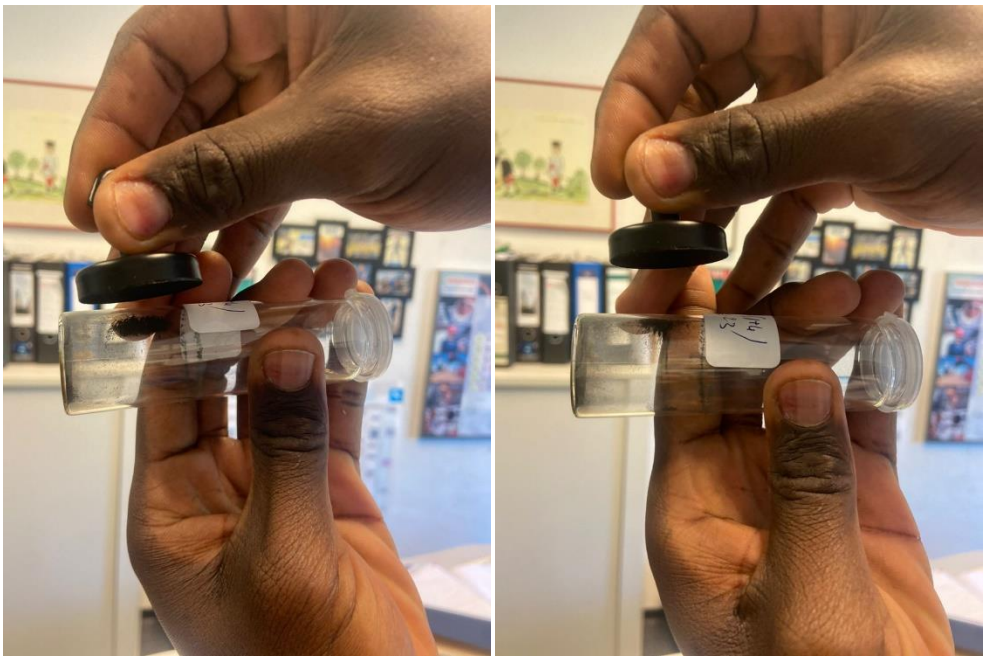

Figure 46: Test of the magnetic property of the obtained particles using a magnet

3.1.5 Magnet collection for industrial solution (Solution C) and Synthetized solution (0.5 mol/l Co)

SEM analysis was performed on two different samples: one derived from an industrial solution (Solution C) and the other synthesized at 0.5 mol/L cobalt concentration using USP at 950°C with magnet collection. The results indicated a multimodal distribution of particles, with Figure 47 showing fewer particles compared to Figure 48. In the industrial solution (Figure 47), particle sizes ranged from 0.194 to 1.101 µm, with a mean size of 0.509 µm. In the synthesized solution (Figure 48), particle sizes ranged from 0.227 to 0.936 µm, with a mean size of 0.538 µm. The presence of smaller particle sizes in both samples may lead to distinct magnetic, mechanical, and thermal properties, influenced by precursor concentration, flow rate, and synthesis conditions. Additionally, the higher concentration of the synthesized solution compared to the industrial solution could have contributed to the observed variations in particle size and properties. The SEM analysis and comparison of particle size distributions offer valuable insights into the material's

characteristics and behavior, relevant to various applications in magnetic, mechanical, and thermal systems.

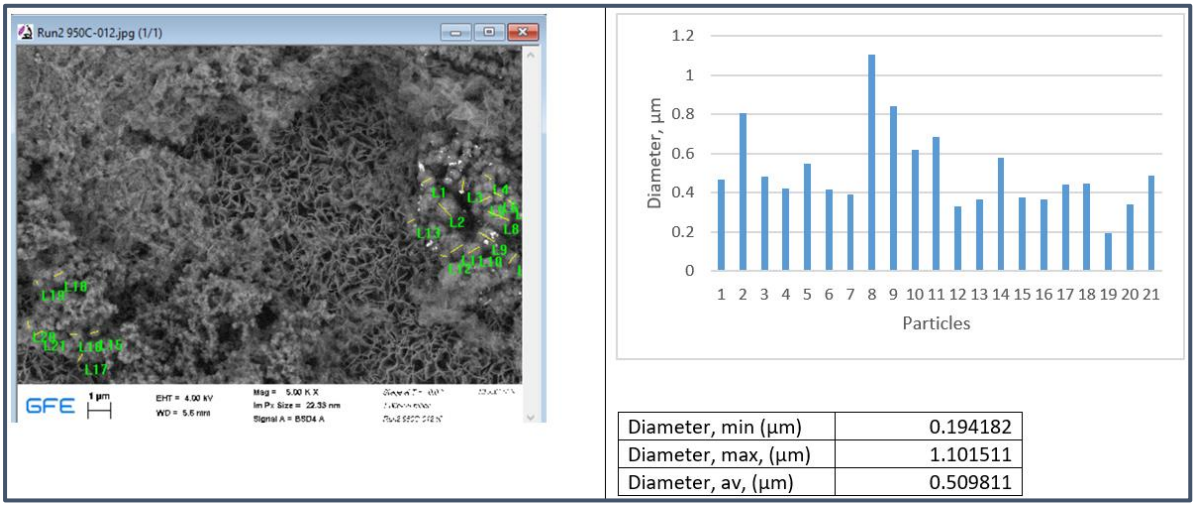

Diameter, min (µm)	0.194182
Diameter, max, (µm)	1.101511
Diameter, av, (µm)	0.509811

Figure 47: Particle size distribution of Cobalt from solution C (Industrial solution) at 950°C

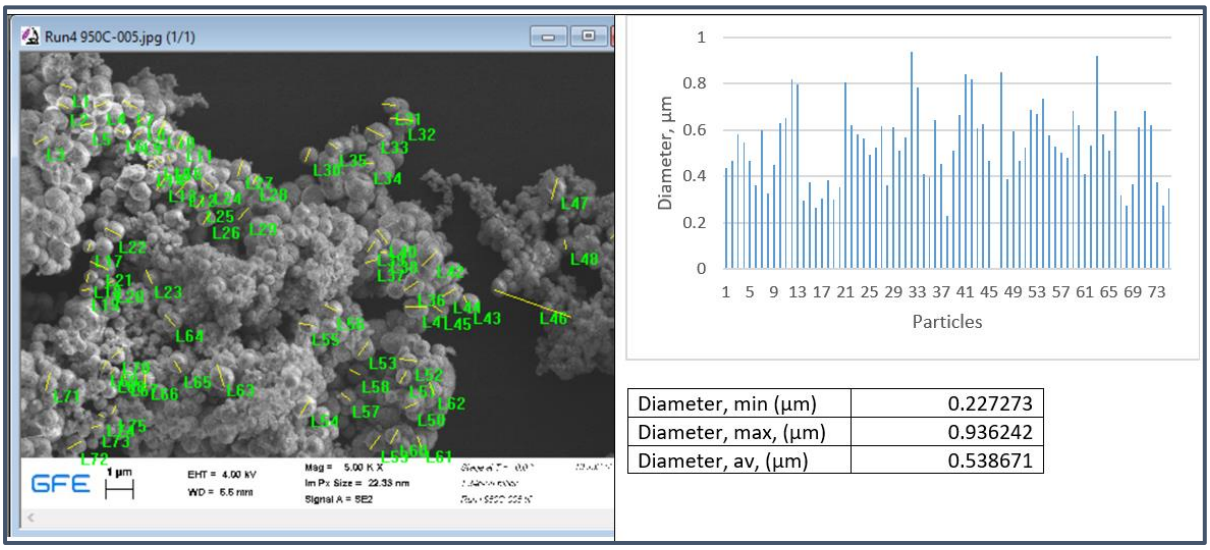

Diameter, min (µm)	0.227273
Diameter, max, (µm)	0.936242
Diameter, av, (µm)	0.538671

Figure 48: Particle size distribution of Cobalt from the synthetic solution of 0.5 mol/l cobalt nitrate at 950°C

3.1.6 XRD analysis result

Figure 49 shows the XRD patterns of the powders prepared at 950ºC, with magnetic separation. The result shows that we obtained cobalt.

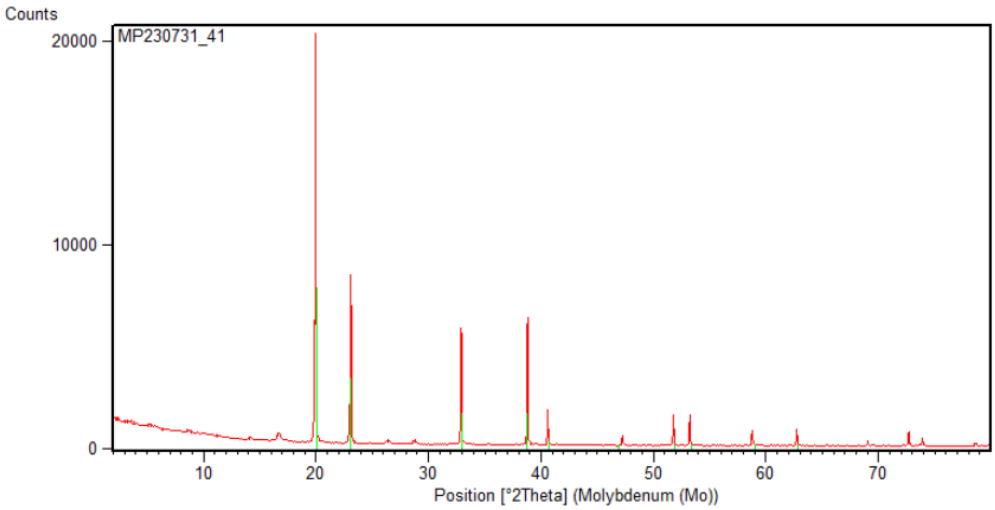

PARTIAL CONCLUSION

In this study, particles produced using the USP-HR method were extensively analyzed through SEM, EDS, and XRD techniques. We investigated the impact of various processing parameters, including temperature, solution concentration, residence time, and particle collection using a magnet.

Our findings reveal that these processing parameters significantly affect the morphology, elemental composition, and crystallinity of the particles. Notably, agglomeration is more pronounced at 600°C compared to 900°C, and increasing the temperature favors the production of spherical cobalt particles. Furthermore, increasing the solution concentration leads to larger particle sizes. A short residence time of 7 seconds during a 2-hour reaction time appears to be the optimal condition for synthesizing cobalt nanoparticles. Spherical cobalt nanoparticles were successfully obtained at 600°C, whereas a longer residence time at 900°C resulted in pronounced agglomeration. The use of magnets for particle collection was explored and proved to be effective, addressing the issue of fine particle release from the outlet pipe. This innovative approach to particle collection holds promise for future applications.

CONCLUSIONS AND PERSPECTIVES

This study explored the potential of synthesizing cobalt powder from a waste solution generated during the leaching of polycrystalline diamond blanks. The investigation involved 21 experimental runs using two distinct reactors with varying residence times (7.19 sec and 23 sec). Ultrasonic spray pyrolysis (USP) was employed to create fine, spherical, nanosized cobalt particles from the waste solution. The aerosol droplets underwent hydrogen reduction within the temperature range of 600 to 950°C, yielding cobalt powder. The volumetric flow rate of 3 l/min (1 l/min Ar, 2 l/min H2) and a 2-hour reaction time were employed.

Results indicated that higher temperatures resulted in increased cobalt production. Furthermore, altering the cobalt concentration in the solution influenced particle size, showing that higher concentration led to larger particles. A short residence time (7.9 seconds) at 900°C was found to be more suitable for cobalt nanoparticle synthesis, with spherical particles ranging from 191.1nm to 1222nm. While the potential for powder collection using a magnet was evident, the limited cobalt powder recovery could be attributed to precursor concentration or magnetic strength insufficiency. Despite successful powder capture, addressing the challenge of powder recovery from the tube is crucial.

Comparing particle size distributions between the industrial and synthesized solutions revealed minimal differences, with average particle sizes of 0.509 μm and 0.538 μm, respectively.

The study's perspective involves extracting cobalt from waste solutions generated during polycrystalline diamond blank leaching for reuse, as depicted in the provided flow chart. While USP and hydrogen reduction demonstrate promise for cobalt nanoparticle recovery, refining the purification process and enhancing magnetic particle collection efficiency are necessary steps forward.

BIBLIOGRAPHIC REFERENCE

[1] Stankovic S., Kamberovic Ž., Friedrich B., Stopic S., Sokic M., Markovic B., Schippers A, 2022. Options for Hydrometallurgical Treatment of Ni-Co Lateritic Ores for Sustainable Supply of Nickel and Cobalt for European Battery Industry from South-Eastern Europe and Turkey. *Metals*, 12, 807.

[2] Ayodeji S., Chinnan M. D., and Katlong A., 2023. Africa's Critical Minerals and the Global Electric Vehicle (EV) Market. African Energy Council report, 12p.

[3] Cobalt Institute, 2021. Cobalt Market Report. Cobalt Institute final report (Zurich). 46p

[4] Pourret, O., Faucon, MP. (2016). Cobalt. In: White, W. (eds) Encyclopedia of Geochemistry. Encyclopedia of Earth Sciences Series. Springer, Cham. https://doi.org/10.1007/978-3-319-39193-9_271-1.

[5] Chandra M., Yu D., Tian Q., and Guo X., 2021. Recovery of Cobalt from Secondary Resources: A Comprehensive Review, *Mineral Processing and Extractive Metallurgy Review*, 43, 22.

[6] Britannica, 2023. Cobalt: Uses, Properties, & Facts. [Online]. Available on: https://www.britannica.com/science/cobalt-chemical-element (accessed May 03, 2023).

[7] Burgex Mining Consultants, 2021. Cobalt: A Resurging Commodity. [Online]. Available on: https://burgex.com/cobalt-a-resurging-commodity/ (accessed May 16, 2023).

[8] Smith C. G., 2001. Always the bridesmaid, never the bride: cobalt geology and resources. *Applied. Earth Science.*, 110, 2, pp. 75–80, Aug. 2001, doi: 10.1179/aes.2001.110.2.75.

[9] Pazik P. M., Chmielewski T., Glass H. J., and Kowalczuk P. B., 2016. World production and possible recovery of cobalt from the Kupferschiefer stratiform copper ore, *E3S Web of Conferences.*, vol. 8, p. 01063. Doi: 10.1051/e3sconf/20160801063.

[10] Siegel F., 2019. Is there enough Cobalt to meet the need for batteries? [Online]. Available on https://blog.energybrainpool.com/en/is-there-enough-cobalt-to-meet-the-need-for-batteries/ (accessed May 16, 2023).

[11] Fisher K. G., 2011. Cobalt processing developments. In Southern African Institute of Mining and Metallurgy. (ed.): 6th Southern African Base Metals Conference. Southern African, pp 237-258

[12] Greg A., 2014. 'Nickel Laterites: The World's Largest Source of Nickel. [Online]. Available on: https://www.geologyforinvestors.com/nickel-laterites/ (accessed Jul. 23, 2023).

[13] Stanković S., Stopić S., Sokić M., Marković B., and Friedrich B., 2020. Review of the past, present, and future of the hydrometallurgical production of nickel and cobalt from lateritic ores. *Metallurgical and Materials Engineering Association of Metallurgical Engineers of Serbia AMES*, 26, no. 2, pp. 199–208.

[14] Stopić S. and Friedrich B., 2020. Recovery of cobalt from primary and secondary materials: An overiew, *Vojnoteh. Glas*, vol. 68, pp. 321–337.

[15] Hara Y. R. S., Kaluba G., Musowoya D., Chikontwe K., Muchindu C., Simfukwe H., Chanda T. P., and Parirenyatwa S., 2020. Leaching of Copper, Cobalt, and Nickel from Complex Ore. In J. Li, M. Zhang, B. Li, S. N. Monteiro, S. Ikhmayies, Y. E. Kalay, J.-Y. Hwang, J. P. Escobedo-Diaz, J. S. Carpenter, and A. D. Brown, (eds.): *Characterization of Minerals, Metals, and Materials.* Zambia, pp 227-236.

[16] Ilyas S., Srivastava R. R., Kim H., Ilyas N., and Sattar R., 2020. Extraction of nickel and cobalt from a laterite ore using the carbothermic reduction roasting-ammoniacal leaching process. *Separation and Purification Technology*, vol. 232, p. 115971.

[17] Sivasakthi P., and Sathaiyan N., 2012. Cobalt Recovery from Waste Catalysts: Petroleum Refining Industry from Gujarat, *Open Journal of Metal*, vol. 02, no. 01, pp. 24–30.

[18] Wolańczyk Z., Rzelewska-Piekut M., Cierpiszewski R., Staszak K., and Regel-Rosocka M., 2020. Hydrometallurgical Recovery of Cobalt(II) from Spent Industrial Catalysts. *Catalysts*, vol. 10, p. 61.

[19] Zeng X., Li J., and Singh N., 2014. Recycling of Spent Lithium-Ion Battery: A Critical Review. *Critical Reviews in Environmental Science and Technology*, vol. 44, no. 10, pp. 1129–1165. Doi: 10.1080/10643389.2013.763578.

[20] Xu J., Thomas H. R., Francis R. W., Lum K. R., Wang J., and Liang B., 2008. A review of processes and technologies for the recycling of lithium-ion secondary batteries. *Journal of Power Sources*, vol. 177, no. 2, pp. 512–527. Doi: 10.1016/j.jpowsour.2007.11.074.

[21] Rarotra S., Sahu S., Kumar P., Kim K.-H., Tsang Y. F., Kumar V., Kumar P., Srinivasan M., Veksha A., and Lisak G., 2020. Progress and Challenges on Battery Waste Management :A Critical Review. *ChemistrySelect*, vol. 5, no. 20, pp. 6182–6193.

[22] Lain M. J., 2001. Recycling of lithium ion cells and batteries. *Journal of. Power Sources*, vol. 97–98, pp. 736–738. Doi: 10.1016/S0378-7753(01)00600-0.

[23] Nan J., Han D., and Zuo X., 2005. Recovery of metal values from spent lithium-ion batteries with chemical deposition and solvent extraction. *Journal of. Power Sources*, vol. 152, pp. 278–284. Doi: 10.1016/j.jpowsour.2005.03.134.

[24] Wang M.-M., Zhang C.-C., and Zhang F.-S., 2016. An environmental benign process for cobalt and lithium recovery from spent lithium-ion batteries by mechanochemical approach. *Waste Management*, vol. 51, pp. 239–244. Doi: 10.1016/j.wasman.2016.03.006.

[25] Dutta D., Kumari A., Panda R., Jha S., Gupta D., Goel S., and Jha M. K., 2018. Close loop separation process for the recovery of Co, Cu, Mn, Fe and Li from spent lithium-ion batteries. *Separation and Purification Technology*, vol. 200, pp. 327–334.

[26] Chen L., Tang X., Zhang Y., Li L., Zeng Z., and Zhang Y., 2011. Process for the recovery of cobalt oxalate from spent lithium-ion batteries. *Hydrometallurgy*, vol. 108, no. 1, pp. 80–86. Doi: 10.1016/j.hydromet.2011.02.010.

[27] Joulié M., Laucournet R., and Billy E., 2014. Hydrometallurgical process for the recovery of high value metals from spent lithium, nickel, cobalt, aluminum oxide based lithium-ion batteries. *Journal of Power Sources*, vol. 247, pp. 551–555.

[28] Swain B., Jeong J., Lee J., Lee G.-H., and Sohn J.-S., 2007. Hydrometallurgical process for recovery of cobalt from waste cathodic active material generated during manufacturing of lithium ion batteries. *Journal of Power Sources*, vol. 167, no. 2, pp. 536–544.

[29] Byun S. Y., Park J. S., Kang J. H., Seo S., Tran T., and Kim M. J., 2021. Recovery of tungsten and cobalt from cemented tungsten carbide wastes using carbonate roasting and water leaching. *Journal of Air Waste Management. Association 1995*, vol. 71, no. 6, pp. 711–720.

[30] British Geological Survey, Bureau de Recherches Géologiques et Minières, Deloitte Sustainability, 2017. Study on the review of the list of critical raw materials. European Commission Final report, Brussels, 92p.

[31] Xi X., Xiao X., Nie Z., Zhang L., and Ma L., 2017. Electrolytic separation of cobalt and tungsten from cemented carbide scrap and the electrochemical behavior of metal ions. *Journal of Electroanalytical Chemestry*, vol. 794, pp. 254–263.

[32] Kießling F., Stopic S., Gürmen S., and Friedrich B., 2020. Recovery of Diamond and Cobalt Powders from Polycrystalline Drawing Die Blanks via Ultrasound Assisted Leaching Process—Part 2: Kinetics and Mechanisms. *Metals*, vol. 10, no. 6, Art. no. 6.

[33] Flowers P., Robinson W. R., Langley R., Theopold K., 2015. Magnetic Properties of Coordination Compounds and Crystal Field Theory. In OpenStax (ed.): *Chemistry*. Houston, Texas, 24-

[34] Encyclopaedia Britannica, 2023. Ferromagnetism: Definition, Cause, Examples, Uses, & Facts. [Online]. Available on: https://www.britannica.com/science/ferromagnetism (accessed Aug. 02, 2023).

[35] Helmenstine A., 2021. List of Magnetic Metals. [Online]. Available on: https://sciencenotes.org/list-of-magnetic-metals/ (accessed Aug. 03, 2023).

[36] BBC, 2023. Filtration. [Online]. Available on: https://www.bbc.co.uk/bitesize/topics/zych6g8/articles/zfwbvwx (accessed Aug. 03, 2023).

[37] Biocyclopedia, 2023. Filtration: Basic laboratory procedures II, Fundamental laboratory techniques. [Online]. Available on: https://biocyclopedia.com/index/chem_lab_methods/filtration.php (accessed Aug. 03, 2023).

[38] Hosansky D., 2023. Electrostatic precipitator: Definition, Diagram, Application Of, & Uses. [Online]. Available on: https://www.britannica.com/technology/electrostatic-precipitator (accessed Aug. 03, 2023).

[39] Bang J. H., and Suslick K. S., 2010. Applications of Ultrasound to the Synthesis of Nanostructured Materials. *Advanced Materials*, vol. 22, no. 10, pp. 1039–1059.

[40] Gürmen S., Stopić S., and Friedrich B., 2006. Synthesis of nanosized spherical cobalt powder by ultrasonic spray pyrolysis. *Materials Research Bulletin*, vol. 41, no. 10, pp. 1882–1890,

[41] Stopić S., Wenz F., Volkov Husovic T., and Friedrich B., 2021. Synthesis of Silica Particles Using Ultrasonic Spray Pyrolysis Method. *Metals*, vol. 11, p. 463.

[42] Majerič P., and Rudolf R., 2020. Advances in Ultrasonic Spray Pyrolysis Processing of Noble Metal Nanoparticles-Review. *Materials*, vol. 13, no. 16, Art. no. 16.

[43] Malvern panalytical X-ray Diffraction (XRD): Overview. [Online]. Available on: https://www.malvernpanalytical.com/en/products/technology/xray-analysis/x-ray-diffraction (accessed May 28, 2023).

[44] Bunaciu A. A., Udriştioiu E. G., and Aboul-Enein H. Y.,2015. X-ray diffraction: instrumentation and applications, *Critical Reviews in Analytical Chemistry*, vol. 45, no. 4, pp. 289–299.

[45] Barbara L Dutrow B. L., Louisiana State University, Christine M. Clark C. M., Eastern Michigan University. X-ray Powder Diffraction (XRD). [Online]. Available on: https://serc.carleton.edu/research_education/geochemsheets/techniques/XRD.html (accessed May 28, 2023).

[46] Jang H. C., Ju S. H., and Kang Y. C., 2010. Characteristics of fine size Fe-Ni alloy powders directly prepared by spray pyrolysis. *Metals and Materials International*, vol. 16, no. 4, pp. 643–647.

[47] Thermofisher Scientific, 2023. SEM EDS. [Online]. Available on: https://www.thermofisher.com/de/de/home/materials-science/chemisem.html (accessed May 28, 2023).

[48] SEMLab, 2023. EDS Analysis. [Online]. Available on: https://www.semlab.com/services/edsanalysis/ (accessed Jun. 05, 2023).

[49] O'Driscoll A., 2023. How SEM/EDS Works and Its Applications in Materials Science. [Online]. Available on: https://www.labmanager.com/product-focus/how-sem-eds-works-and-its-applications-in-materials-science-30255 (accessed May 28, 2023).

[50] Vedantu, 2023. Nanoparticle. [Online]. Available on: https://www.vedantu.com/physics/nanoparticle (accessed Jun. 11, 2023).

[51] Murthy S. K., 2007. Nanoparticles in modern medicine: State of the art and future challenges. *International Journal of Nanomedicine*, vol. 2, no. 2, pp. 129–141.

[52] Azonano, 2013. Iron Cobalt (Fe-Co) Nanoparticles: Properties, Applications. [Online]. Available on: https://www.azonano.com/article.aspx?ArticleID=3333 (accessed Jun. 11, 2023).

[53] Nochehdehi A. R., Thomas S., Revaprasadu N., Grohens Y., and Kalarikkal N., 2020. Biomedical Applications of Iron- and Cobalt-Based Biomagnetic Alloy Nanoparticles. In, Daima H. K., PN N., Ranjan S., Dasgupta N., and Lichtfouse E., (eds.): *Nanoscience in Medicine*, Environmental Chemistry for a Sustainable World, vol. 1 pp. 333–371.

[54] Iravani S. and Varma R. S., 2020. Sustainable synthesis of cobalt and cobalt oxide nanoparticles and their catalytic and biomedical applications. *Green Chemestry*, vol. 22, no. 9, pp. 2643–2661.

[55] Vodyashkin A. A., Kezimana P., Prokonov F. Y., Vasilenko I. A., and Stanishevskiy Y. M., 2022. Current Methods for Synthesis and Potential Applications of Cobalt Nanoparticles: A Review. *Crystals*, vol. 12, no. 2, Art. no. 2.

[56] Leon V., 2018. Cobalt, Lithium-ion Batteries and Social Sustainability. [Online]. Available on: https://www.3blmedia.com/news/cobalt-lithium-ion-batteries-and-social-sustainability (accessed Aug. 03, 2023).

[57] Ocean Minerals LLC, 2023. Cobalt . [Online]. Available on: https://www.omlus.com/ocean-minerals-llc-cobalt/ (accessed Aug. 03, 2023).

[58] Choa Y.-H., Yang J.-K., Kim B.-H., Jeong Y.-K., Lee J.-S., Nakayama T., Sekino T., Niihara K, 2003. Preparation and characterization of metal/ceramic nanoporous nanocomposite powders. *Journal. Magnetism and Magnetic Materials*, vol. 266, no. 1, pp. 12–19.

[59] Shatrova N., Yudin A., Levena V., Dzidziguri E., Kuznetsov D., Perov N., and Issi J.-P., 2017. Elaboration, characterization and magnetic properties of cobalt nanoparticles synthesized by ultrasonic spray pyrolysis followed by hydrogen reduction. *Materials Research Bulletin*, vol. 86, pp. 80–87.

[60] Gurmen S., Ebin B., Stopić S., and Friedrich B., 2009. Nanocrystalline spherical iron–nickel (Fe–Ni) alloy particles prepared by ultrasonic spray pyrolysis and hydrogen reduction (USP-HR). *Journal of Alloys Compound.*, vol. 480, no. 2, pp. 529–533.